UILU-ENG-91-2009

CIVIL ENGINEERING STUDIES

STRUCTURAL RESEARCH SERIES NO. 561

ISSN: 0069-4274

APPROXIMATE TECHNIQUES OF J ESTIMATION APPLICABLE TO PART-THROUGH SURFACE CRACKS

By
MARK T. KIRK
ROBERT H. DODDS, JR.

A Report on a Research Project
Sponsored by the
DAVID TAYLOR RESEARCH CENTER
METALS AND WELDING DIVISION
ANNAPOLIS, MARYLAND,
Research Contract: N61533-90-K-0059

DEPARTMENT OF CIVIL ENGINEERING
UNIVERSITY OF ILLINOIS AT
URBANA-CHAMPAIGN
URBANA, ILLINOIS
AUGUST 1991

The Influence of Weld Strength Mismatch on Crack–Tip Constraint in Single Edge Notch Bend Specimens

By

Mark T. Kirk
Robert H. Dodds, Jr.
Department of Civil Engineering
University of Illinois

A Report on a Research Project Sponsored by the:

DAVID TAYLOR RESEARCH CENTER
METALS AND WELDING DIVISION

Annapolis, Maryland 21402

University of Illinois
Urbana, Illinois
February 1992

50272-101

REPORT DOCUMENTATION PAGE	1. REPORT NO. UILU-ENG-91-2009	2.	3. Recipient's Accession No.

4. Title and Subtitle Approximate Techniques of J Estimation Applicable to Part-Through Surface Cracks	5. Report Date August 1991 6.
7. Author(s) Mark T. Kirk and Robert H. Dodds, Jr.	8. Performing Organization Report No. SRS 561
9. Performing Organization Name and Address University of Illinois at Urbana-Champaign Department of Civil Engineering 205 N. Mathews Avenue Urbana, Illinois 61801	10. Project/Task/Work Unit No. 11. Contract(C) or Grant(G) No. N61533-90-K-0059
12. Sponsoring Organization Name and Address David Taylor Research Center Metal and Welding Division, Code 281 Annapolis, Maryland 21402	13. Type of Report & Period Covered Interim: 1-1-91 to 8-1-91 14.

15. Supplementary Notes

16. Abstract (Limit: 200 words)

This investigation concerns the accuracy with which three different estimation schemes predict the variation of applied J with applied strain for semi-elliptical surface cracks. The three estimation schemes considered were a weight function technique proposed by Bhandari, a modification of the EPRI estimation scheme proposed by Ainsworth, and Turner's Engineering-J design curve. Each of these techniques is simple enough to employ in design, the most arduous calculation required being that needed to determine the linear elastic stress intensity factor. Accuracy of the estimation schemes was assessed by comparing J predictions to finite element results for three small semi-elliptical surface cracks in a moderately hardening steel loaded in either pure tension or pure bending. The results obtained indicate that, for applied strains up to three times the yield strain, both the weight function and the modified EPRI schemes under estimate applied J by between 23% and 83% depending on the applied strain level. Conversely, Turner's Engineering-J design curve provides accurate or conservative (i.e. over) estimates of applied J in both tension and bending provided total crack size is less than 3% of the total cross sectional area and maximum crack depth is less than 25% of the plate thickness. Application to larger and deeper cracks loaded in tension is not recommended as the design curve does not conservatively account for net section yielding in these situations. The design curve can still be applied in bending to cracks of size up to 7% of the total cross sectional area. However, the degree of conservatism inherent in this application may be considered excessive in certain situations.

17. Document Analysis a. Descriptors

Surface Cracks, Approximate Techniques, Fracture Mechanics, Finite Elements

b. Identifiers/Open-Ended Terms

c. COSATI Field/Group

18. Availability Statement	19. Security Class (This Report)	21. No. of Pages
Release Unlimited	UNCLASSIFIED	41
	20. Security Class (This Page) UNCLASSIFIED	22. Price

(See ANSI-Z39.18)

OPTIONAL FORM 272 (4-77)
Department of Commerce

Approximate Techniques of J Estimation Applicable to Part-Through Surface Cracks

By

Mark T. Kirk
Robert H. Dodds, Jr.
Department of Civil Engineering
University of Illinois

A Report on a Research Project Sponsored by the:

DAVID TAYLOR RESEARCH CENTER
METALS AND WELDING DIVISION

Annapolis, Maryland 21402

University of Illinois
Urbana, Illinois
August 1991

ABSTRACT

This investigation concerns the accuracy with which three different estimation schemes predict the variation of applied J with applied strain for semi–elliptical surface cracks. The three estimation schemes considered were a weight function technique proposed by Bhandari, a modification of the EPRI estimation scheme proposed by Ainsworth, and Turner's Engineering–J design curve. Each of these techniques is simple enough to employ in design, the most arduous calculation required being that needed to determine the linear elastic stress intensity factor. Accuracy of the estimation schemes was assessed by comparing J predictions to finite element results for three small semi–elliptical surface cracks in a moderately hardening steel loaded in either pure tension or pure bending. The results obtained indicate that, for applied strains up to three times the yield strain, both the weight function and the modified EPRI schemes under estimate applied J by between 23% and 83% depending on the applied strain level. Conversely, Turner's Engineering–J design curve provides accurate or conservative (i.e. over) estimates of applied J in both tension and bending provided total crack size is less than 3% of the total cross sectional area and maximum crack depth is less than 25% of the plate thickness. Application to larger and deeper cracks loaded in tension is not recommended as the design curve does not conservatively account for net section yielding in these situations. The design curve can still be applied in bending to cracks of size up to 7% of the total cross sectional area. However, the degree of conservatism inherent in this application may be considered excessive in certain situations.

ACKNOWLEDGMENTS

This report was prepared as part of the Surface Ship and Submarine Materials Block under the sponsorship of I. L. Caplan (David Taylor Research Center, Code 011.5). The work of the first author was performed in the Civil Engineering Department at the University of Illinois as part of an extended term training program. The work supports DTRC Program Element 62234N, Task Area RS345S50.

Computational support and reproduction of this report were made possible by the David Taylor Research Center, Contract No. N61533–90–K–0059.

TABLE OF CONTENTS

LIST OF TABLES

LIST OF FIGURES

1. INTRODUCTION AND OBJECTIVE

Modern computational techniques and computers allow calculation of the applied driving force to fracture (applied J) for complex section shapes, loadings, and crack shapes to a very high degree of precision given adequate time, expertise, and financial resources. Typically, these calculations are performed using the finite element method. This approach, and its attendant accuracy, is appropriate for a research environment. However, its use in a design setting is often either inappropriate (i.e. the accuracy is unwarranted given uncertainties in other design variables) or impossible (i.e. the time required to complete the necessary calculations is excessive due to the large number of different cases that must be considered). Consequently, numerous investigators have proposed "J–Estimation Schemes" as an alternative to detailed finite element calculations. The simplicity of these approaches permits rapid assessment of the effect of cracks on structural integrity, making them attractive for design use. In this investigation, three different estimation schemes are evaluated for how accurately they predict the applied J for part–through semi–elliptical surface cracks. Accuracy is assessed by comparing estimated J values to those calculated using the finite element technique.

2. ESTIMATION SCHEMES EVALUATED

2.1 Weight Function Technique

Bhandari, et al. [1] proposed that weight function techniques, commonly used to estimate linear elastic stress intensity factors from *uncracked* body stress distributions, could be applied to J estimation. J is evaluated as follows:

$$J = \frac{K_\gamma^2}{E'} \tag{2.1.1}$$

where

$K_\gamma = \sqrt{K_\sigma \cdot K_\epsilon}$

K_σ stress intensity resulting from application of nominal (uncracked body) stresses, acting on and normal to the crack location, to the crack in a weight function analysis

K_ϵ stress intensity resulting from application of nominal pseudo–stresses of magnitude $\epsilon E'$ (strain • modulus), acting on and normal to the crack location, to the crack in a weight function analysis

E' elastic modulus, $= E$ in plane stress and $= E/(1-\nu^2)$ in plane strain

ν Poisson's ratio

The K values in eqn. (2.1.1) are determined by a weight function technique. This requires numerical integration of the following equation:

$$K = \int_{CRACK\ AREA} F(P,P') \cdot \sigma(\gamma,\theta)\ dA \tag{2.1.2}$$

where

$F(P,P') = \dfrac{\sqrt{2\sin\theta}}{(\pi\gamma)^{1.5}}$, all terms are defined in Figure 1

$\sigma(\gamma,\theta)$: for K_σ = the stress variation over the crack location in the uncracked body; for K_ϵ = the pseudo-stress ($\epsilon E'$) variation over the crack location in the uncracked body
(These stresses and strains are determined by elastic–plastic finite element analysis of the uncracked body.)

Strictly, the weight function (F) in eqn (2.1.2) is appropriate for analysis of three dimensional cracks with straight fronts. It is applied here to an approximate analysis of a semi-elliptical crack. In linear analysis, Marriott [2] demonstrated that use of this weight function produces an error of at most 9% for any semi-elliptical crack.

2.2 Modified EPRI Approach

Ainsworth [3] proposed a J estimation formula based on reference stress concepts common to creep analysis [4] that considerably simplifies the *Engineering Approach for Elastic – Plastic Fracture Analysis* developed by the Electric Power Research Institute (EPRI) [5]. The EPRI approach uses the Ramberg–Osgood constitutive relation

$$\frac{\epsilon}{\epsilon_o} = \frac{\sigma}{\sigma_o} + a\left(\frac{\sigma}{\sigma_o}\right)^n \tag{2.2.1}$$

where

σ_o	yield strength
ϵ_o	yield strain, $= \sigma_o/E$
E	Young's modulus
a	material constant
n	material strain hardening coefficient

The EPRI J estimation formulas partition J into elastic and plastic parts which are summed to determine the total J. These equations have the general form

$$J_{total} = J_{el} + J_{pl} \tag{2.2.2a}$$

$$J_{el} = \frac{K^2(a_{eff})}{E'} \tag{2.2.2b}$$

$$J_{pl} = a\sigma_o\epsilon_o c h_1(a/t, n)\left[\frac{P}{P_o}\right]^{n+1} \tag{2.2.2c}$$

where

K elastic stress intensity factor calculated using the applied load and a plastic zone corrected crack length

$$a_{eff} = a + \frac{1}{\beta\pi}\left(\frac{n-1}{n+1}\right)\left(\frac{K}{\sigma_o}\right)^2 \frac{1}{1 + (P/P_o)^2}$$

β 2 for plane stress and 6 for plane strain

E' elastic modulus, $= E$ in plane stress and $= E/(1-\nu^2)$ in plane strain

ν Poisson's ratio

c characteristic structural length

h_1 non–dimensional material and geometry dependent function

P applied load

P_o characteristic load

Equation (2.2.2) is of little use in design because an elastic–plastic finite element analysis of the cracked structure is needed to define the h_1 function. Further, the plastic part of J is quite sensitive to the strain hardening exponent because it appears as a power $(n+1)$. As eqn. (2.2.1) is difficult to fit to actual uniaxial stress–strain data, particularly for materials with a pronounced yield plateau, the numeric value of n is often uncertain. This introduces large uncertainties in the value of J_{pl}. To alleviate these difficulties, Ainsworth found that replacing the characteristic load P_o with the limit load (P_L) calculated for a rigid – plastic material of yield strength σ_o minimizes the variation of h_1 with strain hardening coefficient[1]. This considerably simplifies calculation of h_1, for if h_1 is independent of n, then it can be approximated using the geometry corrections contained within ordinary linear elastic stress intensity factor solutions. These solutions are widely available for planar [7] as well as surface–crack geometries [8]. Ainsworth found that

1. Limit loads can be estimated readily by bounding techniques or, for small cracks, by elastic–plastic finite element analyses of the uncracked structure. Compendia of limit load solutions are also available [6].

$$h_1 = \frac{\mu K^2(a)}{c\sigma_{ref}^2} \tag{2.2.3}$$

where

μ 1 in plane stress and 0.75 for plane strain

σ_{ref} $\sigma_o(P/P_L)$

P_L limit load for a rigid – plastic material of yield strength σ_o

Introduction of the reference stress in eqn. (2.2.3) further simplifies the EPRI approach as it eliminates the dependence of J_{pl} on the strain hardening coefficient. These modifications allowed Ainsworth to express eqn. (2.2.2) as follows:

$$J_{total} = J_{el} + J_{pl} \tag{2.2.4a}$$

$$J_{el} = \frac{K^2(a_{eff})}{E'} \tag{2.2.4b}$$

$$J_{pl} = \mu K^2(a)\left[\frac{\epsilon_{ref} P_L}{\sigma_o P} - \frac{1}{E}\right] \tag{2.2.4c}$$

where

ϵ_{ref} strain corresponding to an applied stress of σ_{ref} on the uni–axial stress–strain curve

Applied J can be calculated using eqn. (2.2.4) provided the uniaxial stress–strain curve, a stress intensity factor (K) solution, and a limit load solution are available for the conditions of interest. Newman and Raju report stress intensity factors for part–through semi elliptical cracks in simple geometries [8]. If idealization to a simple geometry is not possible, simple techniques can be used to estimate K [2]. The great majority of cracks considered in design are small, removing at most a few percent of the total load bearing cross section. Consequently, the presence of the crack need not be considered in limit load calculations.

2.3 Turner's Engineering–J Design Curve

Turner [9] described a J design curve based on the results of elastic plastic, plane strain, finite element analyses of shallow cracks ($a/W \leq 0.1$) in a variety of different geometries and loading configurations. The design curve estimates J as a function of an effective structural (nominal) strain that depends upon notch depth. Separate equations are used depending on the global deformation response:

Region I **LEFM:** A load controlled region wherein plastic deformation is confined to very near the crack tip. Linear Elastic Fracture Mechanics defines the J – strain relation in this region.

$$J = \left(\frac{e}{e_y}\right)^2 G_y \qquad \text{for } e/e_y \leq 0.85 \qquad (2.3.1a)$$

Region II **NSY:** A region in which Yielding occurs through the Net Section of the structure. J increases rapidly with strain in this region.

$$J = 5\left[\left(\frac{e}{e_y}\right) - 0.7\right] G_y \qquad \text{for } 0.85 \leq e/e_y \leq 1.2 \qquad (2.3.1b)$$

Region III **GSY:** Yielding occurs in the Gross Section of the structure, it is not restricted to the crack tip–region. The rate at which J increases with increasing strain falls off once GSY is achieved.

$$J = 2.5\left[\left(\frac{e}{e_y}\right) - 0.2\right] G_y \quad \text{for } e/e_y > 1.2 \qquad (2.3.1c)$$

In these equations;

e	remote (nominal) strain for the uncracked body
e_y	yield strain, $= E/\sigma_y$
σ_y	yield stress
E	Young's modulus
G_y	K_{Iy}^2/E
K_{Iy}	$\sigma_y \sqrt{a}\, Y$
a	maximum crack depth
Y	linear elastic shape factor

This relation is presented graphically in Figure 2. Equation (2.3.1) indicates that, as for Ainsworth's modified EPRI approach, a linear elastic stress intensity factor solution for the geometry of interest is needed to employ Turner's design curve. However, no limit load solution is required.

2.4 Summary

Table 1 summarizes the information needed to employ each of these methods. Additionally, each of these estimation schemes require that analysis results be post–processed in some way. Of the three considered, post–processing is most complex for the weight function analysis,

a FORTRAN code of several hundred lines being required. Post–processing of analysis results for the other two estimation schemes can be performed using a hand calculator or a spreadsheet.

3. REFERENCE J SOLUTIONS FOR SEMI–ELLIPTICAL SURFACE CRACKS IN TENSION AND BENDING

Finite element models are used to obtain reference solutions for semi elliptical surface cracks loaded in both remote tension and remote bending. Figure 3 shows the geometry and crack sizes evaluated. A constitutive model characteristic of a high strength steel with moderate strain hardening was employed, as illustrated in Figure 4. The following sections describe the finite–element modeling details, numerical techniques for computing J–integral values, and results of linear analyses to examine the adequacy of the mesh refinement. The 3–D models employed a displacement based formulation with the small geometry change approximation. The level of mesh refinement employed in the computations provides sufficiently accurate resolution of the global deformation (load, load–line displacement, and CMOD) and the macroscopic fracture parameters (J and $CTOD$). However, this refinement was insufficient to permit pointwise comparison of the crack–tip strain and stress fields needed for the development of scaling procedures, such as those recently established for SE(B) specimens which fail by transgranular cleavage [10]. This more detailed study would require meshes with 2–3 times the number of nodes and elements. Numerical computations were performed with the POLO–FINITE software [11] operating on an engineering workstation.

3.1 Element Grids and Solution Procedure

Symmetry conditions enabled consideration of only one–quarter of the full specimen in the finite–element model, as shown in Figure 5 for Crack 1. Meshes for the other two cracks were similarly refined. The element mesh was generated with the aid of ORMGEN [12] and the PATRAN [13] solids modeling system. The mesh contained 4377 nodes and 856 20–node isoparametric elements. Figure 5 indicates the level of mesh refinement in the crack region. Seven elements were defined along the crack front ($0 \leq \phi \leq \pi/2$) with a thin layer of elements adjacent to the free surface. Four concentric rings of polygonal elements (eight elements per ring) surrounded the crack tip at each point along the front. The innermost ring contained eight, 20–node elements each collapsed into a wedge with side nodes retained in

the midpoint position. Initially coincident nodes along the crack front were left unconstrained to permit blunting. This model provides singular displacement gradients of order $1/r$ (r = radial distance from crack tip) in the principal normal planes along the crack front (due to the incomplete quadratic functions of the serendipity element, the strength of the singularity varies between corner nodes along the front but is $1/r$ at the corner nodes). The crack–tip elements had a side length $L = 0.013$ in ($L/a = 0.05$). A reduced order of Gaussian quadrature (2x2x2) performed satisfactorily for tension loading but full (3x3x3) integration is required to prevent development of zero–energy modes for bending.

The nonlinear material response was described by incremental plasticity (J_2 flow theory) with a Mises yield surface, associated flow rule, and isotropic hardening. A piecewise–linear representation of the engineering stress–strain curve was adopted. A radial–return algorithm with subincrementation [13, 14] was employed to integrate the constitutive rate equations. This procedure generally provides the most accurate updating of the elastic–plastic stress state corresponding to a specified strain increment.

Displacement constraints to impose the symmetry conditions were applied over the $X=0$ and $Z=0$ planes. Separate analyses were conducted for remote tension and bending loads. Four–point loading was used to impose pure bending on the crack plane. Tensile loading was modeled by applying a uniform axial stress applied over the remote end ($Z = 5.7$–in). For each type of loading, variably sized increments were applied to the model. The use of load, rather than displacement, control suppresses the numerical unloadings that can occur with an incremental (path dependent) plasticity model. The consistent tangent stiffness matrix for the structure corresponding to the radial return integration procedure was updated once for each residual load iteration. The solutions usually required 2–3 equilibrium iterations to reduce the Euclidean norm of the residual loads to below 0.3% of the norm of the applied nodal loads.

3.2 Evaluation of J and CTOD

Analogous with approaches developed for 2–D cracked bodies, a 3–D J–integral parameter, $J_{local}(s)$, was employed to characterize the intensity of stress and strain locally along the curved crack front for Mode I conditions. Given the current lack of analytical solutions defining the asymptotic near tip field in 3–D, $J_{local}(s)$ was defined as the pointwise energy release per unit

area of crack extension, which can be derived using only mechanical energy balance arguments.

For quasistatic loading of stationary cracks, the mathematical expression defining the energy flux at a point s along a line discontinuity is [15],

$$J_{local}(s) = \lim_{\Gamma_\epsilon \to 0} \int_{\Gamma_\epsilon} [Wn_1 - \sigma_{ij} \frac{\partial u_i}{\partial x_1} n_j] \, d\Gamma \tag{3.2.1}$$

where

W	stress–work density
Γ_ϵ	a vanishingly small contour lying in the principal normal plane X_1–X_2 at s
n	a unit normal vector to Γ_ϵ
σ_{ij}	Cartesian stress component in the crack front coordinate system
u_j	Cartesian displacement component in the crack front coordinate system

With the limiting process imposed on Γ, this expression is applicable for general material behavior with arbitrary thermo–mechanical loading and defines the local energy release rate for Mode I crack extension. For a two–dimensional, nonlinear elastic body with the crack extending in the X_1 direction, the above expression reduces to Rice's J–integral [16].

For finite–element computations, numerical integration over vanishingly small contours at the crack front requires very accurate resolution of strain and stress fields and is thus undesirable. To overcome this problem, Domain Integral (DI) methods [17, 18] have been derived by applying the divergence theorem to eqn. (3.2.1). This produces an equivalent integral defined over a finite volume enclosing some portion of the crack front. Domain integrals exhibit volume independence in the same manner that Rice's 2–D J–integral exhibits contour or path independence. While integration over the crack–front elements cannot be avoided, the weight function which appears in the volume integral (i.e. a virtual crack extension) can be defined to minimize the contribution from crack–front elements. In the present computations, the domain integral was evaluated over four volumes defined at corner node locations along the crack front. Excluding the innermost volume, which contained only the crack–front elements, the typical variation of J_{local}(s) values between volumes was less than 3–4%; the largest variation occurring under very extensive plastic deformation.

The use of degenerate 20–node elements along the crack front provides a convenient means to extract CTOD values from displacements of the initially coincident nodes. The

CTOD was taken as the separation of the crack faces at the location where two rays, drawn at right angles to each other from the current crack tip, intercept the crack faces. This procedure is commonly known as the Rice 90° intercept method.

3.3 Linear Analysis to Assess Adequacy of Mesh Refinement

The adequacy of the finite element meshes for these part–through semi elliptical surface cracks was examined through a linear analysis to compute the variation of stress–intensity factor along the crack front. Midside nodes of the collapsed crack–tip elements were positioned at the quarter point to model a $1/\sqrt{r}$ strain and stress singularity. Coincident nodes at each location along the crack front were constrained to have equal displacements. Stress–intensity factors were derived from J using

$$K_I = \sqrt{EJ/(1-\nu^2)} \tag{3.3.1}$$

The present estimates for K_I are compared with the computational results of Raju and Newman [19] in Figure 6. The stress–intensity factors agree within 3–4% at all points along the crack front. Based on this comparison, the level of mesh refinement shown in Figure 5 was considered acceptable for the nonlinear analysis to determine J and $CTOD$ along the crack front.

4. RESULTS AND DISCUSSION

4.1 Comparison of Finite Element Results with J Estimates

Figure 7 shows the variation of J with applied strain and crack front location (ϕ) for the smallest crack (crack area / total cross sectional area = 0.9%) subjected to both remote tension and remote bending. The maximum J (and $CTOD$) develops at the location of maximum crack depth, $\phi = 90°$, in tension but at $\phi = 31°$ in bending. The next largest crack (crack area / total cross sectional area = 3.2%) exhibits similar response. However, for the largest crack considered (crack area / total cross sectional area = 7.4%), the maximum J develops at the location of maximum crack depth in both tension and bending. Tables in Appendix A document the variation of J with position along the crack front for all three cracks modelled.

In this study, the maximum J around the crack front from the finite element analyses is compared to J values calculated at the maximum depth location using the various estimation schemes, because, without the prior knowledge of the finite element results, it would be

unreasonable to expect the maximum J to occur at any location other than at the point of maximum depth. Such information could not be inferred from linear elastic K solutions, for example [8]. The following guidelines were used to compare J values determined by the estimation schemes to the finite element J values:

1. Results are presented for applied strains up to seven times the yield strain. However, when the accuracy of the various estimation schemes is considered, attention is restricted to applied strains of three times yield and lower. Consideration of more extreme overloads in design would be rare. Further, if such a severe event were to be considered, the consequences of failure would likely warrant a more detailed analysis.
2. An estimation scheme is considered "accurate" if it predicts J to within 15% of the finite element value. Over estimates of applied J at a given strain are considered acceptable as use of such values will result in a conservative design. Under estimates of applied J exceeding 15% were not considered acceptable.

Figures 8, 9, and 10 compare the finite element results to J values calculated using the various estimation schemes for remote tensile loading. Each figure presents results for a different crack size. These results indicate that both the weight function and the modified EPRI approach significantly underestimate the applied J for all three surface cracks considered. For applied strains between one and three times the yield strain, the modified EPRI approach under estimates applied J by 23% to 74%, while the weight function approach under estimates applied J by 46% to 83%. Neither of these approaches appear capable of properly tracking J in net section yielding, both transition directly from a J–strain response characteristic of linear elastic conditions to one characteristic of gross–section yielding. Conversely, Turner's Engineering–J design curve contains an explicit provision for net section yielding which tracks the variation of J with strain from the finite element solutions. However, the design curve assumes that a transition to gross section yielding behavior occurs once the applied strain exceeds the yield strain by 20%. As large cracks never transition to gross section yielding, the design curve can be applied conservatively to flaws that are small in proportion to the cross–sectional area. The data in Figures 8 through 10 indicate that, for materials with equal or greater strain hardening capacity to the one investigated here, the upper limit on crack size for conservative design curve applicability is

- maximum crack area = 3% of cross–section

- maximum crack depth = 25% of thickness

For materials with a lower strain hardening capacity, these limits would have to be made more restrictive because lower strain hardening promotes strain localization and, thereby, net section rather than gross section yield.

Figures 11, 12, and 13 compare the finite element results to J values calculated using the various estimation schemes for remotely applied bending. Again both the weight function and the modified EPRI approach generally underestimate applied J. For applied strains between one and three times the yield strain, the modified EPRI approach under estimates applied J by 22% to 44%, while the weight function approach under estimates applied J by 41% to 67%. The only exception to this general observation is that the modified EPRI approach provides a fairly accurate estimate of the variation of J with strain for the largest crack considered (Figure 13). Turner's Engineering–J design curve generally provides better estimates than either the weight function or the modified EPRI approach. Most significantly, at least for strains below three times the yield strain, design curve estimates of applied J are always above the finite element values (i.e. conservative). For the two smaller cracks (Figures 11 and 12), the magnitude of this over prediction is at most 27% of the actual value for applied strains of 3 times the yield strain or less. The design curve also conservatively predicts J for the largest crack considered (Figure 13), but to a much greater extent (almost a factor of two at $e/e_y = 3$). The plastic hinge formed in bending fully yields the crack plane, thus preventing net–section yield and the tendency for the design curve to underestimate applied J, as observed for tensile loading of the largest crack. If crack size is restricted as follows

- maximum crack area = 3% of cross–section
- maximum crack depth = 25% of thickness

Turner's Engineering–J design curve can be used to obtain estimates of applied J slightly above the actual applied J (i.e. conservative) for surface cracks loaded in bending. Further, the design curve can be conservatively applied to surface cracks of greater area (up to 7.4% of the total cross–section). However, this amount of J over–estimation may be considered excessive in some situations.

4.2 Comments on Ainsworth's Modified EPRI Approach

Miller and Ainsworth [20] report good agreement between predictions using Ainsworth's modified EPRI approach and finite element analyses of planar crack geometries [5].

However, the data presented in Figures 8 through 13 indicate that the modified EPRI approach has insufficient accuracy when applied to part–through surface cracks. Predictions of the *J*–strain relationship for part through surface cracks using the modified EPRI approach fail to predict the correct shape of the curve in tension. Further, the rate of *J* increase with strain in gross section yielding is under predicted for both tension and bending. These inadequacies are discussed separately in the following paragraphs.

The inability of the modified EPRI approach to predict the shape of the *J* – strain relation in tension is due to the changing deformation patterns that develop in a part–through surface cracked plate. Dodds and Read [21] observed these patterns experimentally using a birefringent coating applied to a surface cracked plate of A710 steel. They found that different global yielding patterns correspond to different slopes on a plot of *J* vs. remote strain for strains above yield, as illustrated schematically in Figure 14. However, the modified EPRI approach predicts a single value for the slope of the *J*–strain relation at strains above yield. The slope is fixed by the stress intensity factor and limit load solutions used (eqn. 2.2.4), which depend on the crack size and component geometry. Thus, a straightforward application of the modified EPRI approach to a part–through surface crack does not predict a *J*–strain relation having multiple post–yield slopes.

The finite element results in Figures 8 through 13 show that once significant yielding occurs, *J* increases more rapidly with increasing applied strain than predicted by the modified EPRI approximation using stress intensity factor and limit load solutions for a part–through surface crack. Plasticity on the crack plane effectively alters the crack geometry. The loss of stiffness in yielded material causes a part–through surface crack to behave more like a through crack. Figure 15 illustrates this concept. As shown in Figure 16, through crack estimates of *J* vs. strain based on the modified EPRI approach better approximate the gross section yield slope determined by finite element analysis of part–through surface cracks than the part–through crack based estimates did. This trait is characteristic of three–dimensional surface cracks, but not of two–dimensional through cracks. It seems unlikely that a prediction using the modified EPRI approach based on stress intensity factor and limit load solutions appropriate to the initial crack geometry can correctly predict the *J*–strain response of a part–through surface crack.

5. SUMMARY AND CONCLUSIONS

The following conclusions may be drawn from the information developed in this investigation. These conclusions apply specifically to a moderately strain hardening material (post yield hardening modulus = elastic modulus / 84) for applied strains up to three times the yield strain.

1. The weight function and modified EPRI J estimation schemes significantly under estimate J for semi elliptical surface cracks that range in size between 0.9% and 7.4% of the total cross sectional area for both remote tension and bending loads. Under estimation magnitude ranged from 23% to 83% of the actual J value. Consequently, these estimation schemes have no general utility for design.
2. Turner's Engineering–J design curve provides accurate or conservative (i.e. over) estimates of applied J in both tension and bending provided total crack size is less than 3% of the total cross sectional area and maximum crack depth is less than 25% of the plate thickness. Application to larger and deeper cracks loaded in tension is not recommended as the design curve does not conservatively account for net section yielding in these situations. The design curve can still be applied in bending to cracks of size up to 7% of the total cross sectional area. However, the degree of conservatism inherent in this application of the may be considered excessive in certain situations.

Table 1: Summary of material data and analysis requirements for the various J estimation schemes.

Name of J Estimation Scheme	Material Data Required	Analysis Required
Weight Function	Elastic constants Stress–strain curve	Elastic plastic of uncracked structure
Modified EPRI	Elastic constants Stress–strain curve	Elastic of cracked structure to determine K_I Limit Load
Design Curve	Elastic constants Yield stress	Elastic of cracked structure to determine K_I

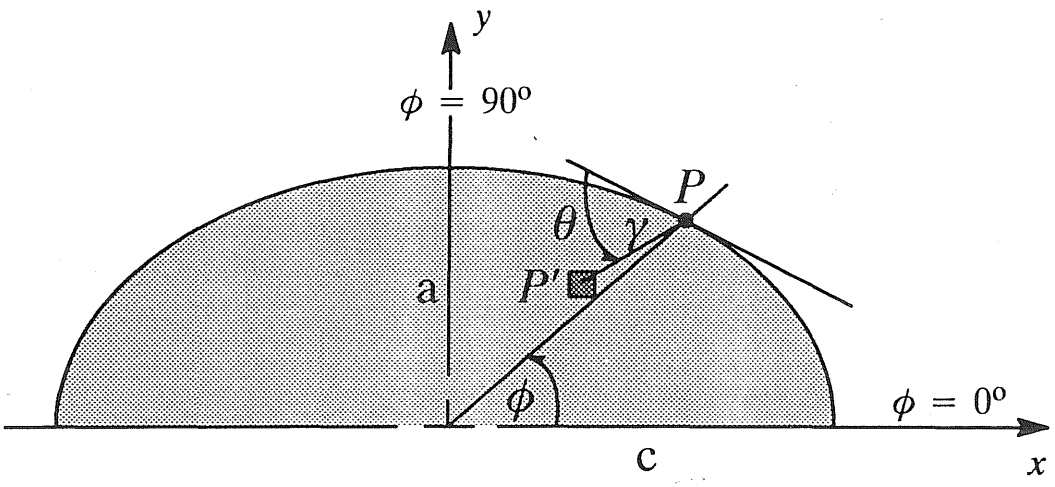

Figure 1: Definition of terms for equation 2.1.2.

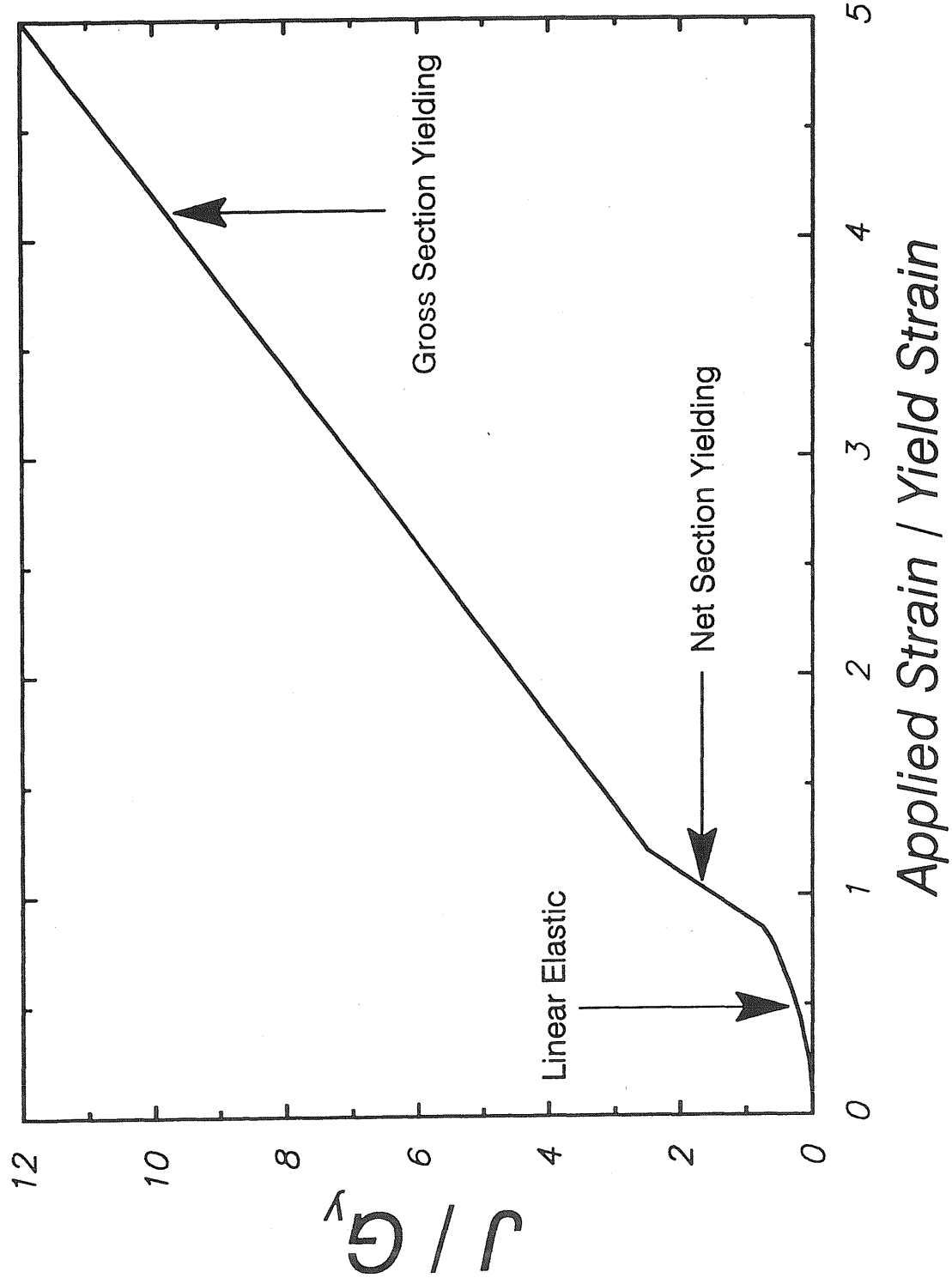

Figure 2: Turner's Engineering–J design curve.

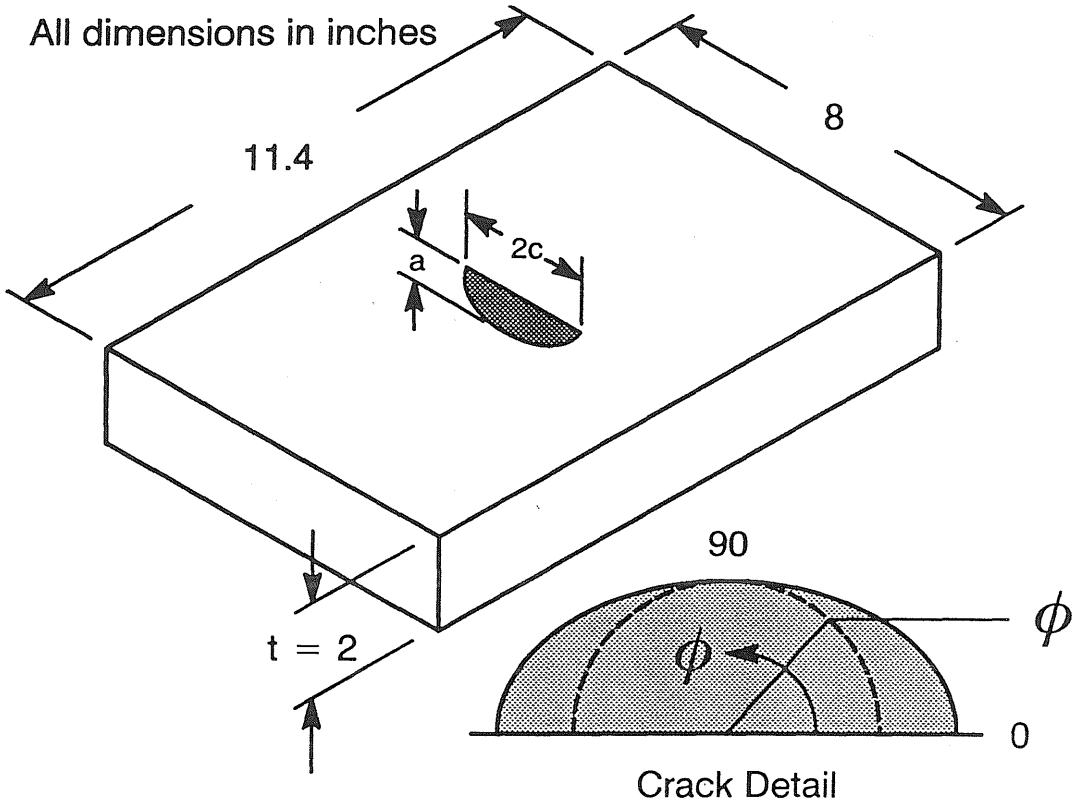

	Crack 1	Crack 2	Crack 3
Depth (a) [inches]	0.26	0.50	0.50
Length (2c) [inches]	0.68	1.30	3.00
Depth / Thickness (a/t)	0.13	0.25	0.25
Aspect Ratio (2c/a)	2.62	2.60	6.00
Crack Area [sq-in]	0.14	0.51	1.18
Crack Area / Total Cross Sectional Area	0.9%	3.2%	7.4%

Figure 3: Surface cracks analyzed.

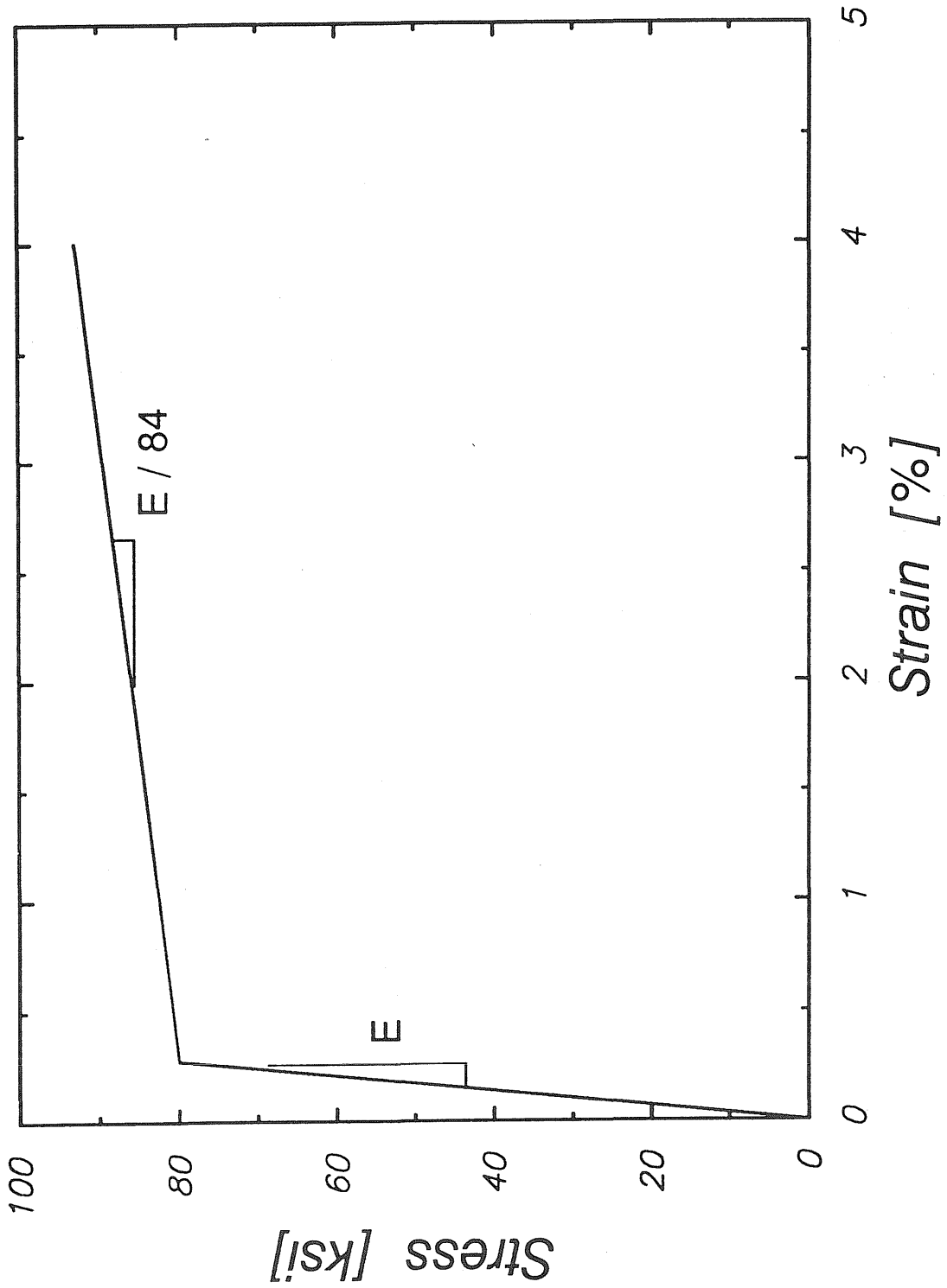

Figure 4: Uniaxial stress–strain curve used for surface crack calculations.

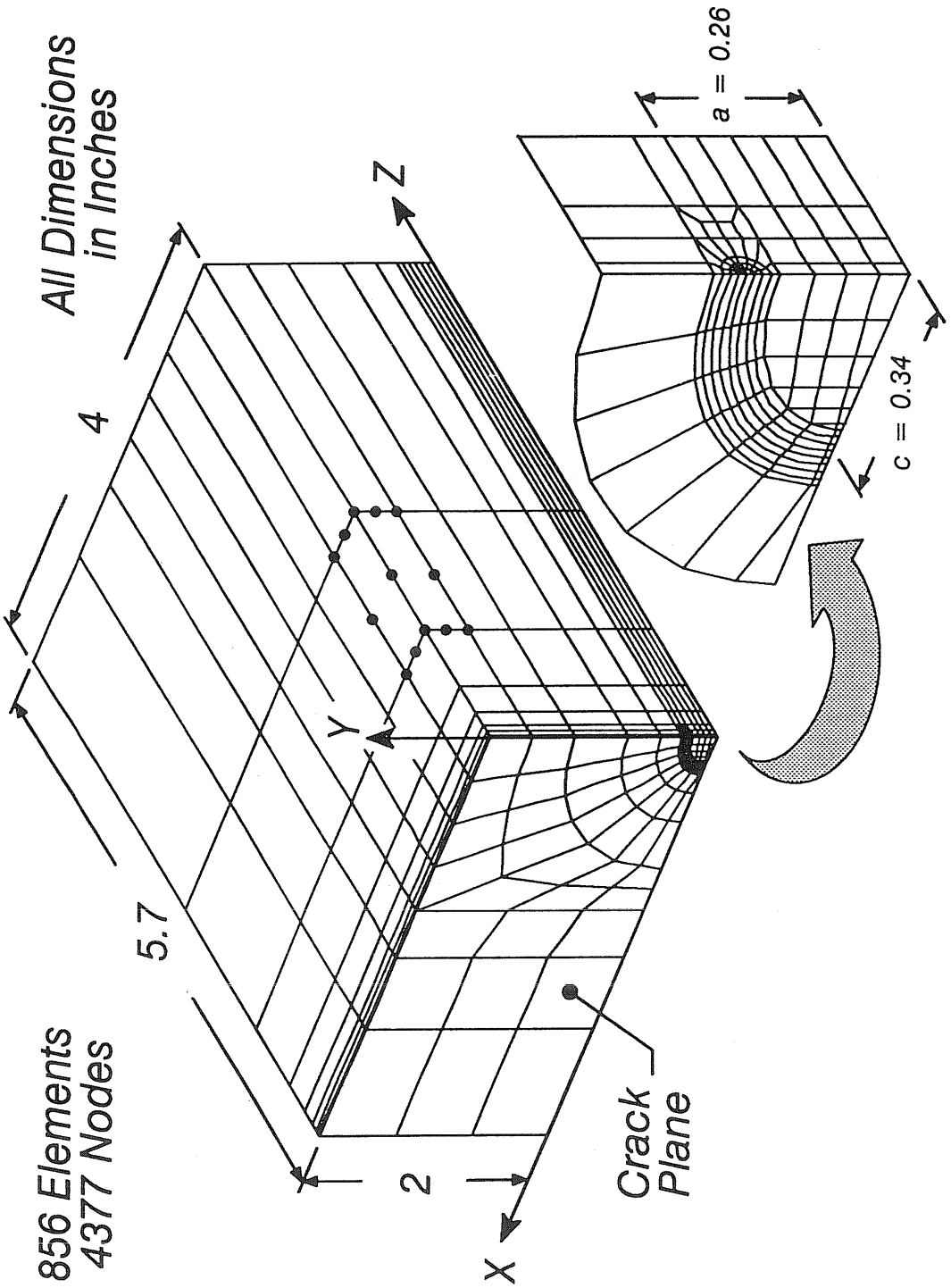

Figure 5: Quarter symmetric finite element mesh for analysis of Crack 1.

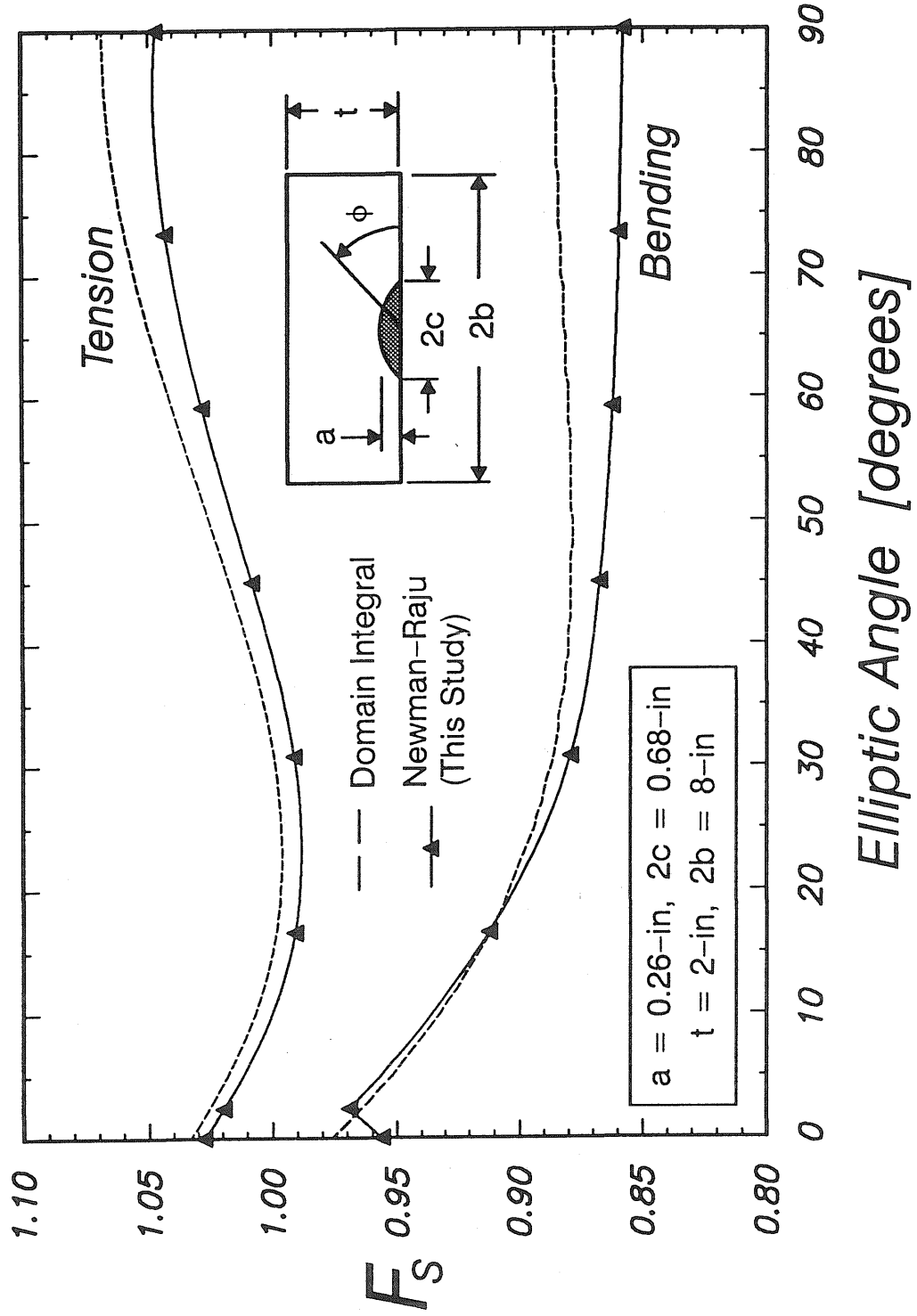

Figure 6: Comparison of K_I prediction for semi–elliptical surface Crack 1 from finite element computation with results due to Newman and Raju [8].

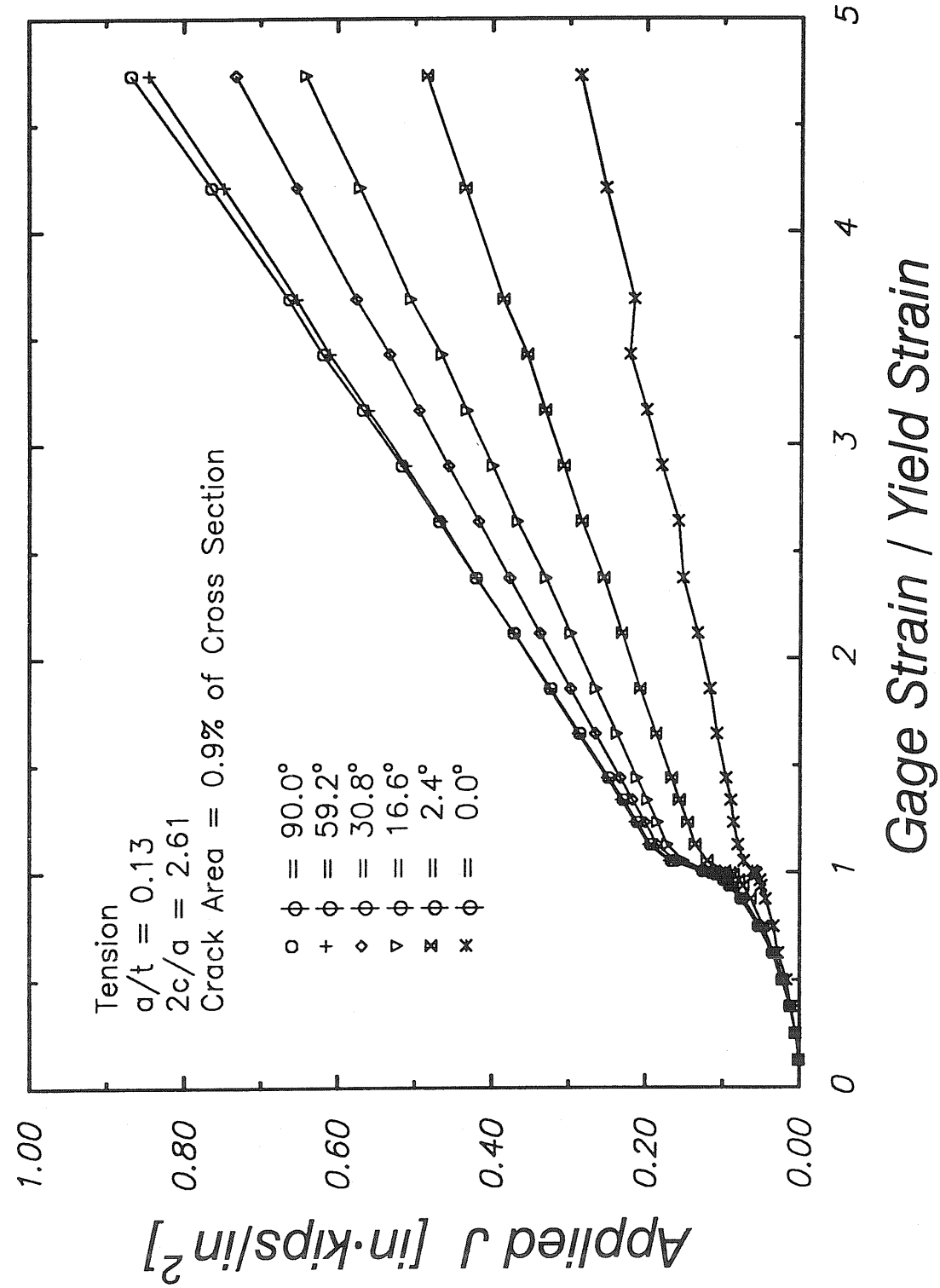

Figure 7a: *J* vs. applied strain determined by finite element analysis for Crack 1 loaded by remote tension.

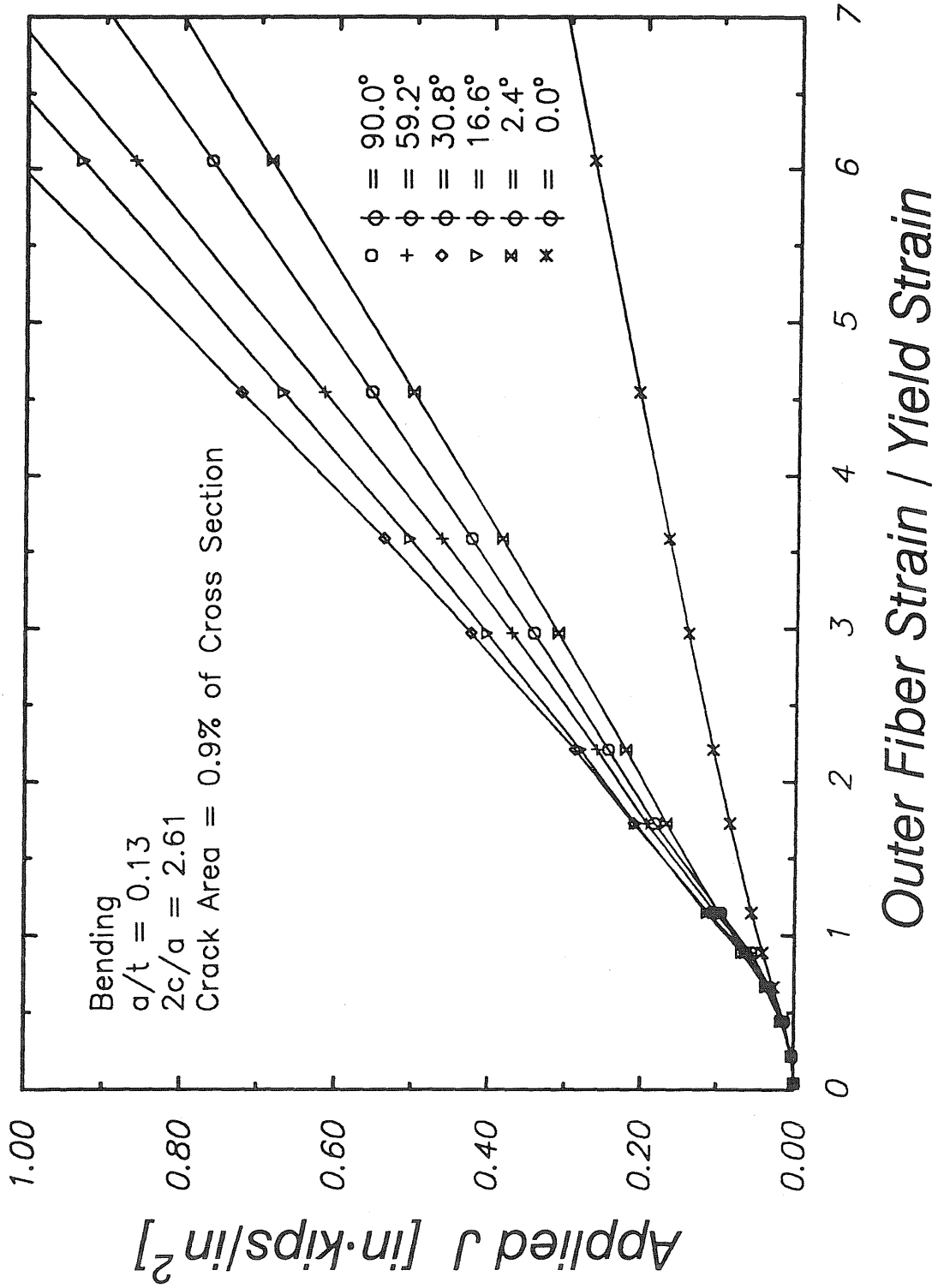

Figure 7b: *J* vs. applied strain determined by finite element analysis for Crack 1 loaded by remote bending.

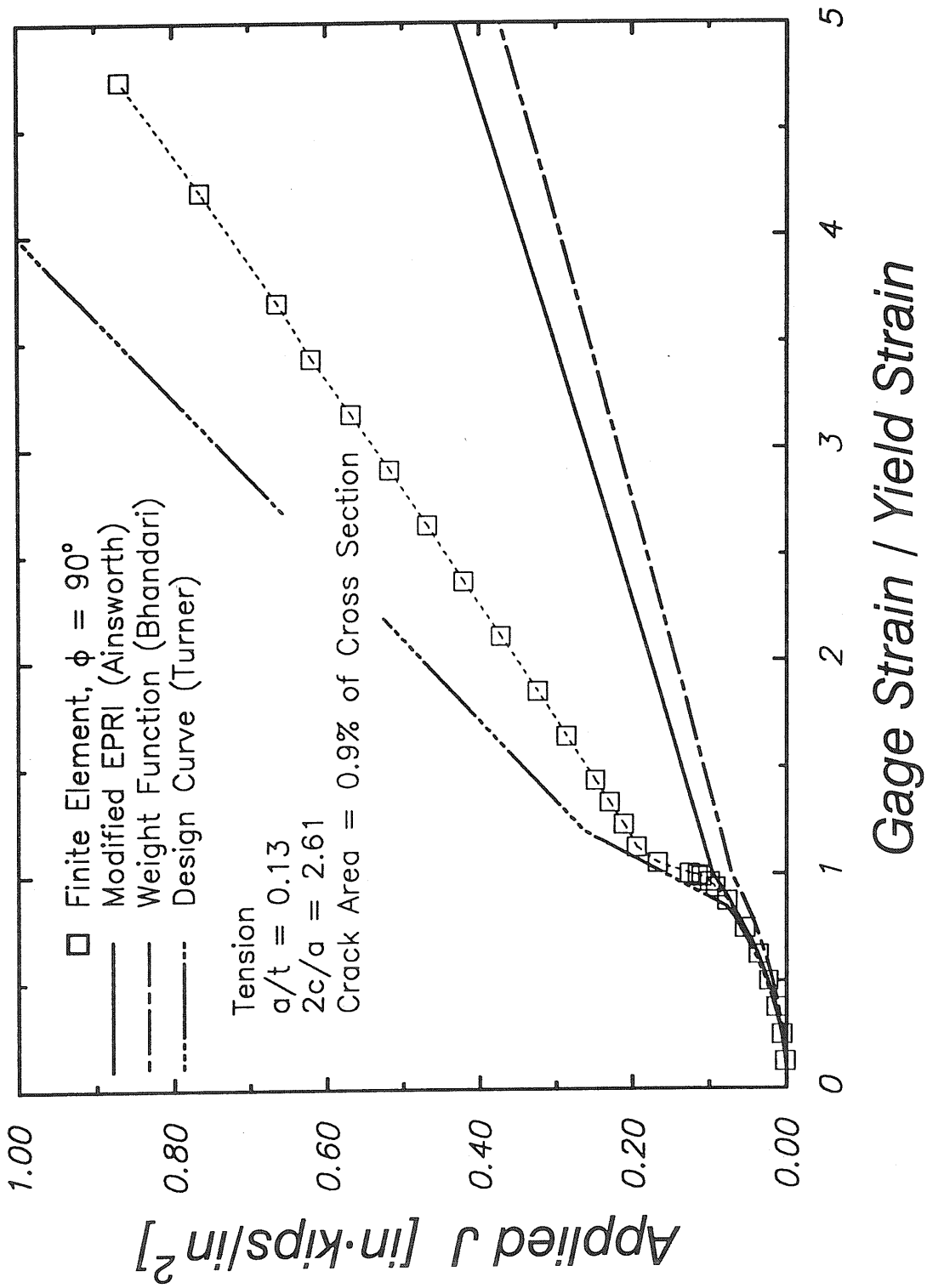

Figure 8: Comparison of approximate J estimates to finite element results for Crack 1 subjected to remote tension loading.

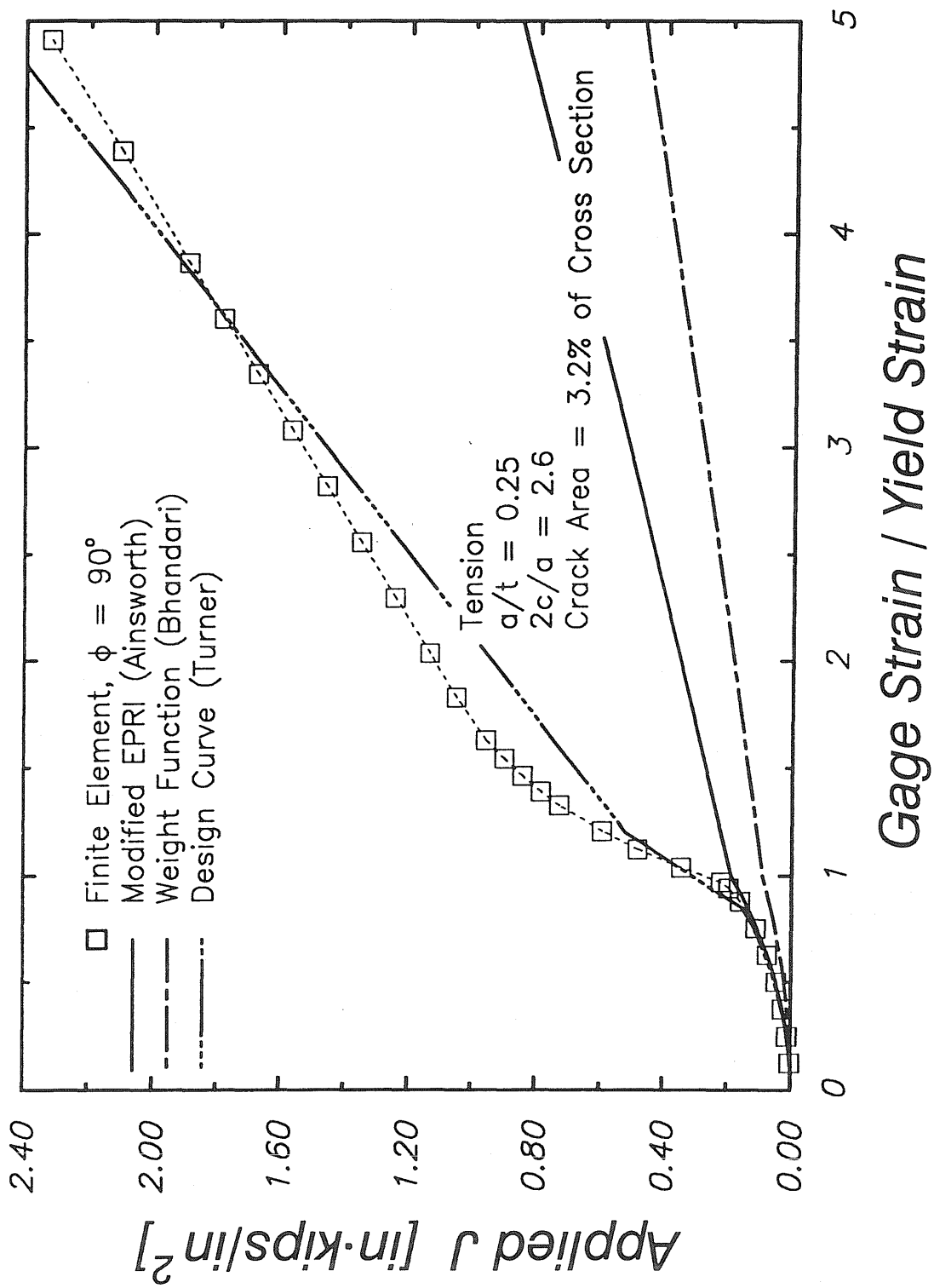

Figure 9: Comparison of approximate J estimates to finite element results for Crack 2 subjected to remote tension loading.

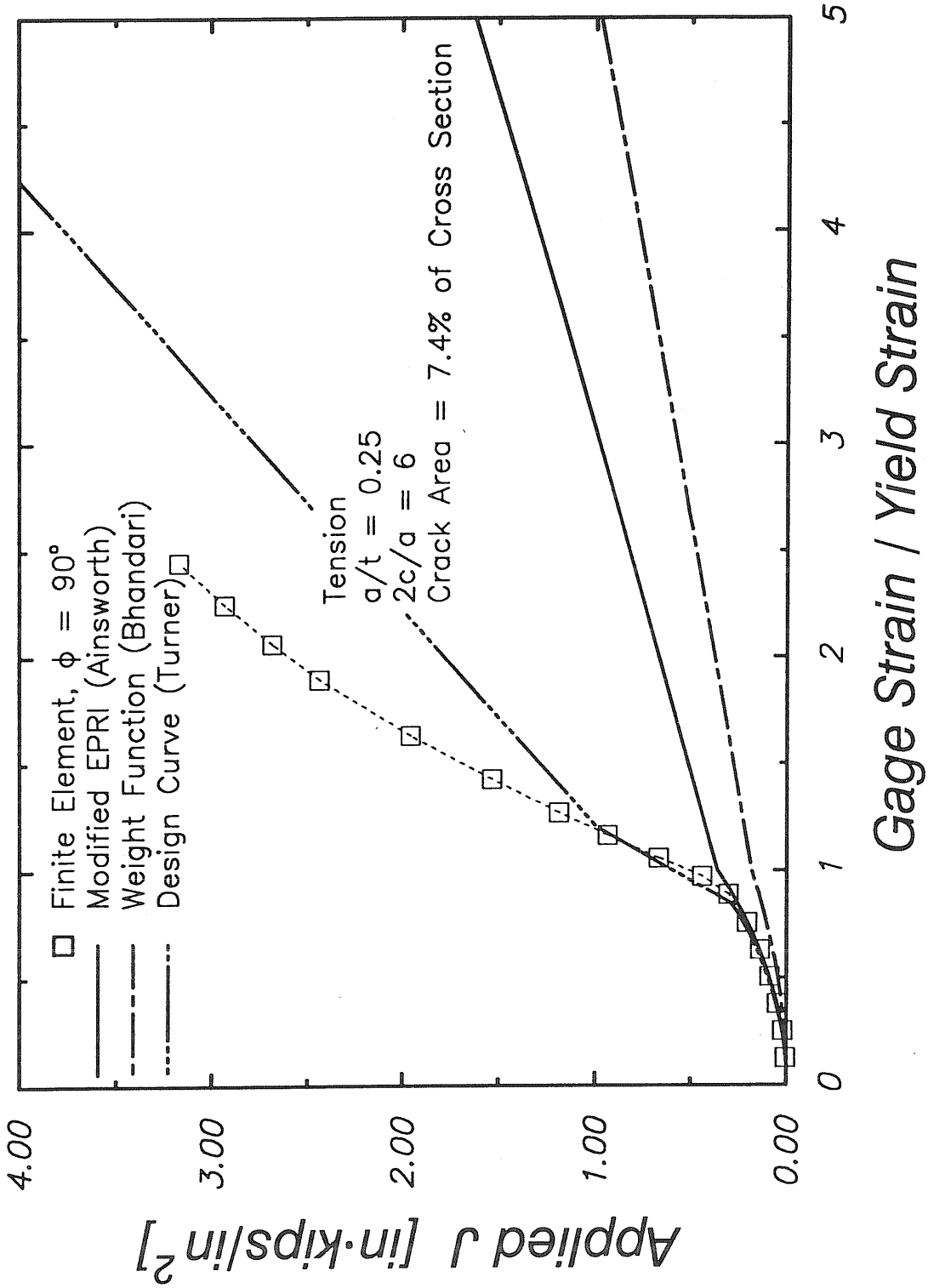

Figure 10: Comparison of approximate J estimates to finite element results for Crack 3 subjected to remote tension loading.

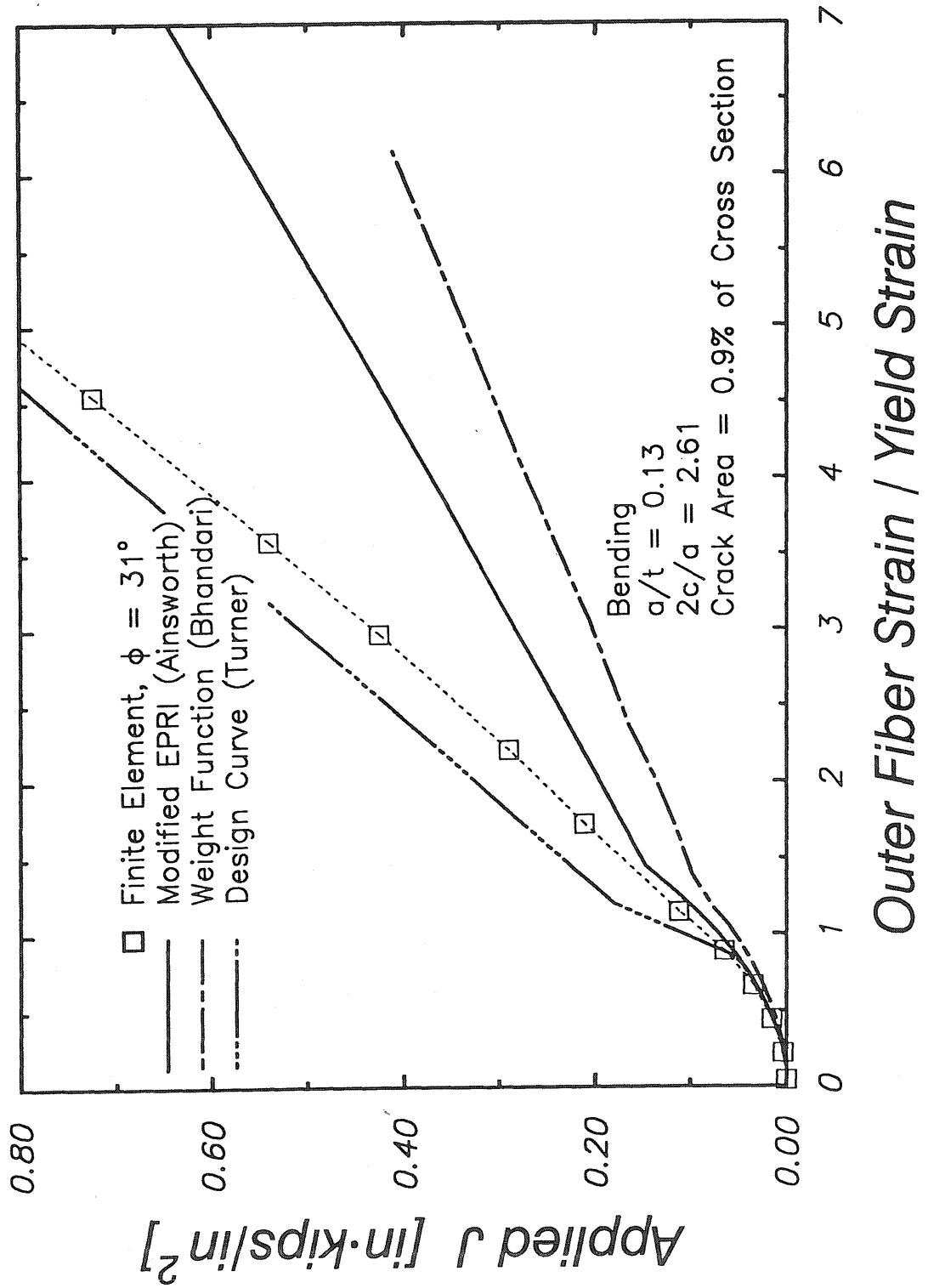

Figure 11: Comparison of approximate J estimates to finite element results for Crack 1 subjected to remote bending loads.

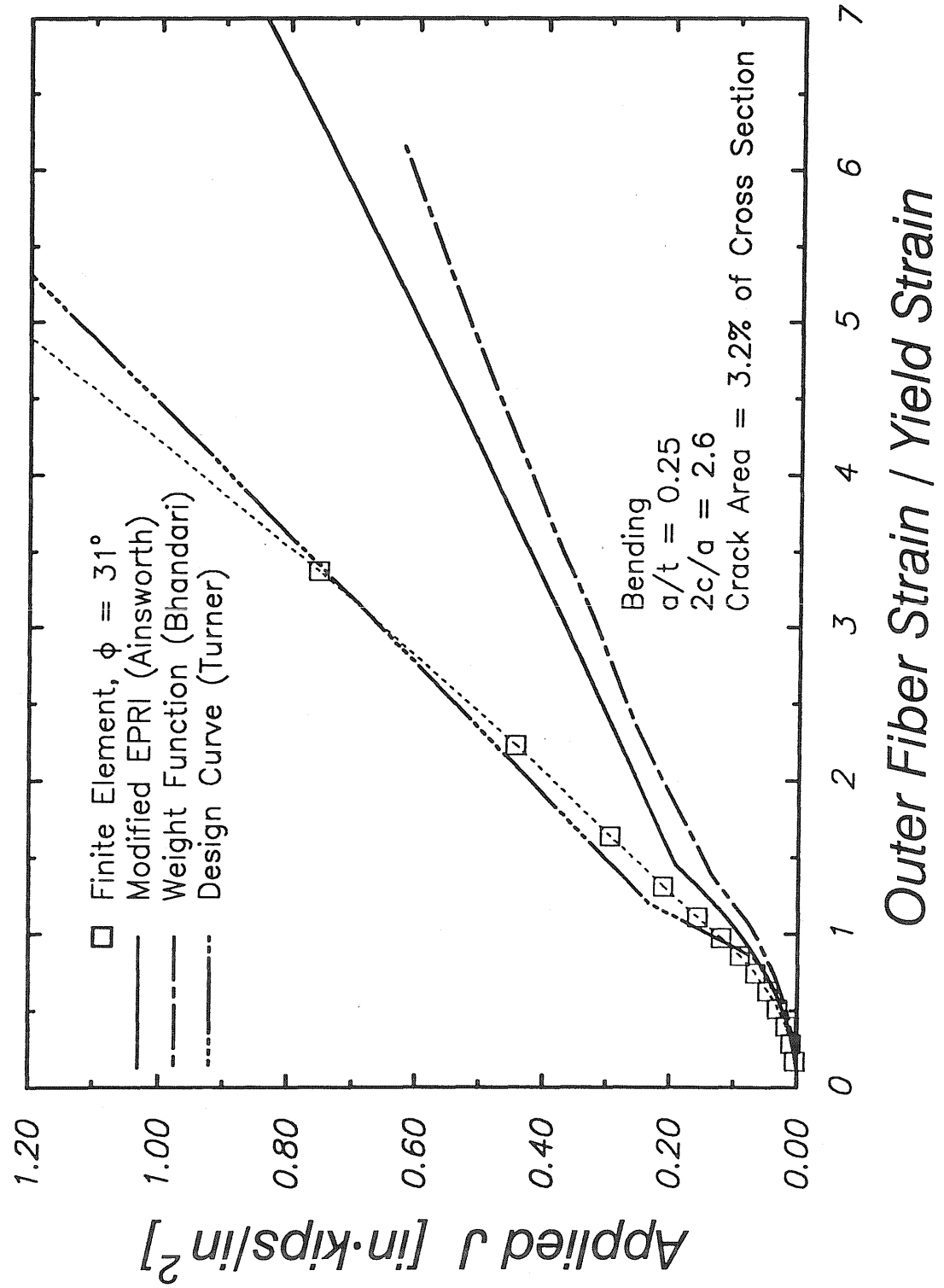

Figure 12: Comparison of approximate J estimates to finite element results for Crack 2 subjected to remote bending loads.

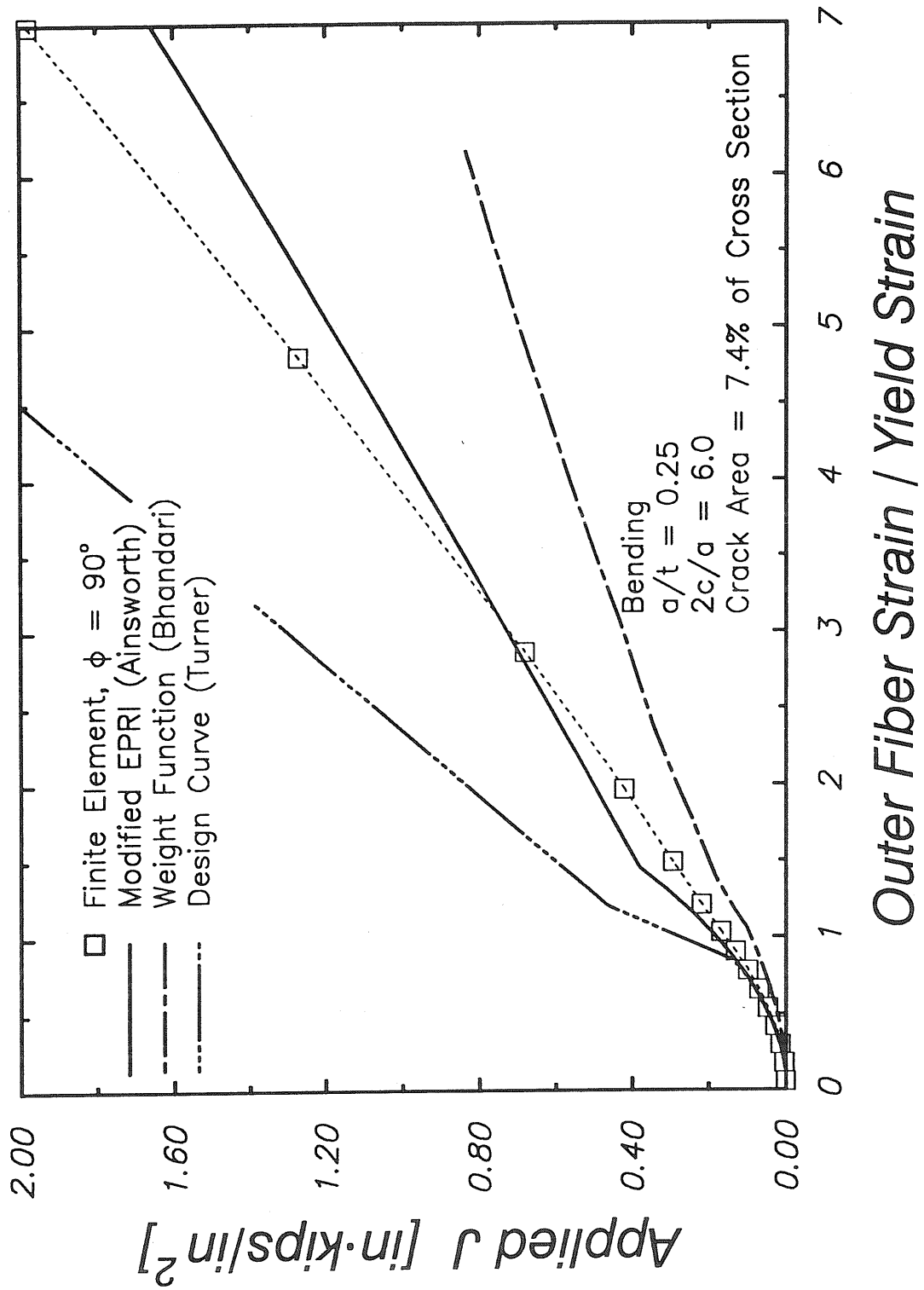

Figure 13: Comparison of approximate *J* estimates to finite element results for Crack 3 subjected to remote bending loads.

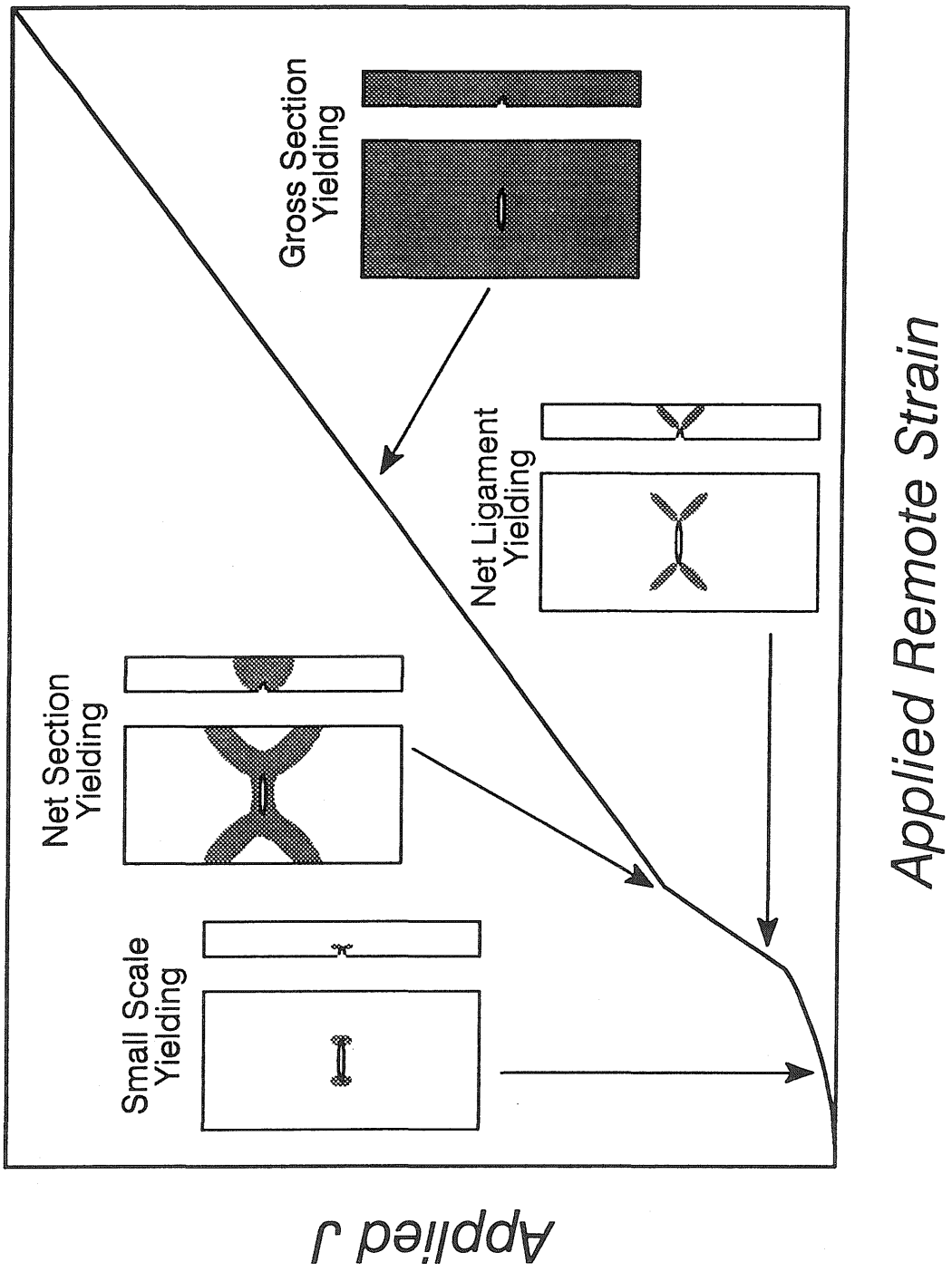

Figure 14: Deformation patterns characteristic of a part–through surface crack loaded in tension [21].

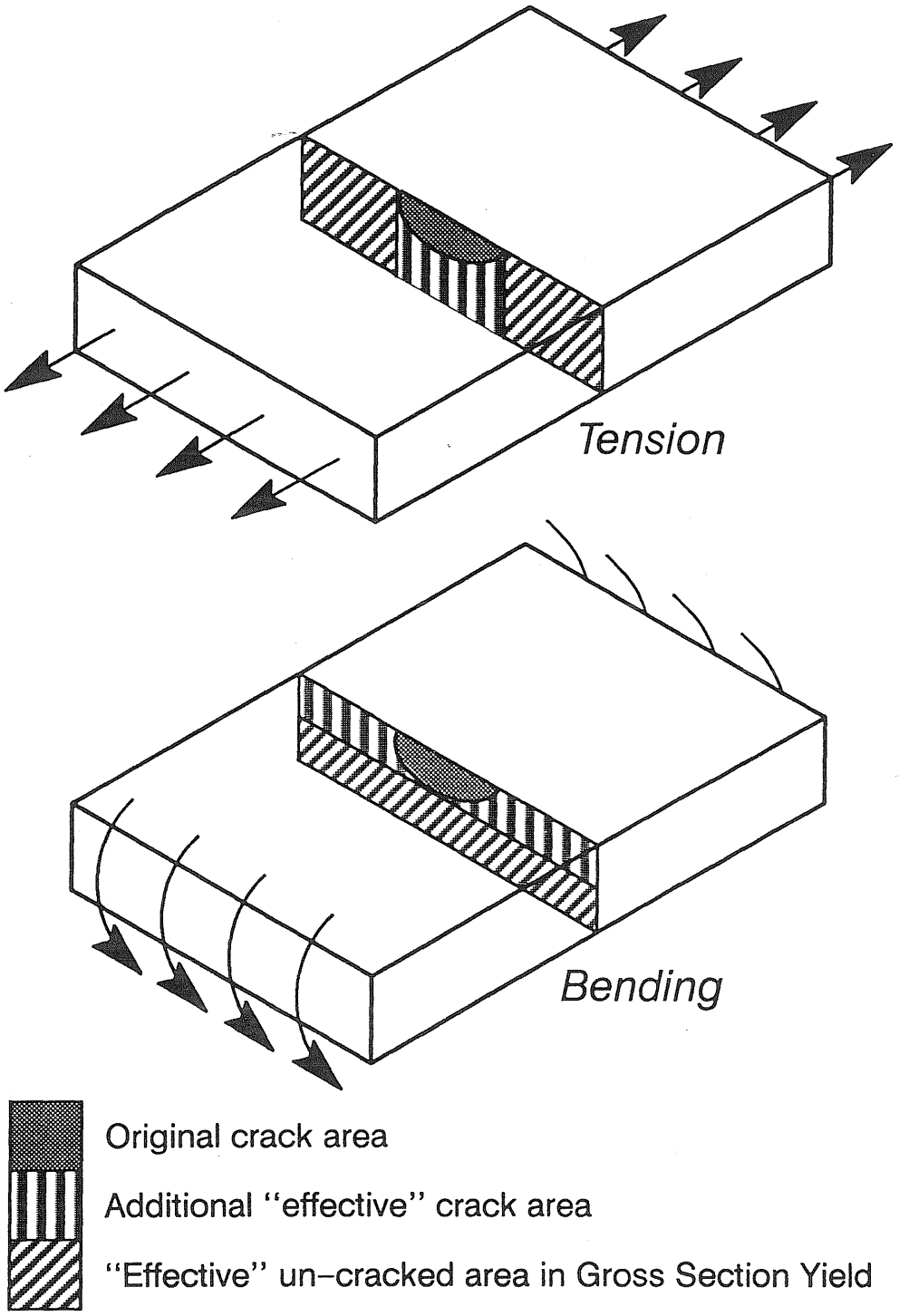

Figure 15: Effective through cracks that form from part-through cracks under gross section yielding conditions.

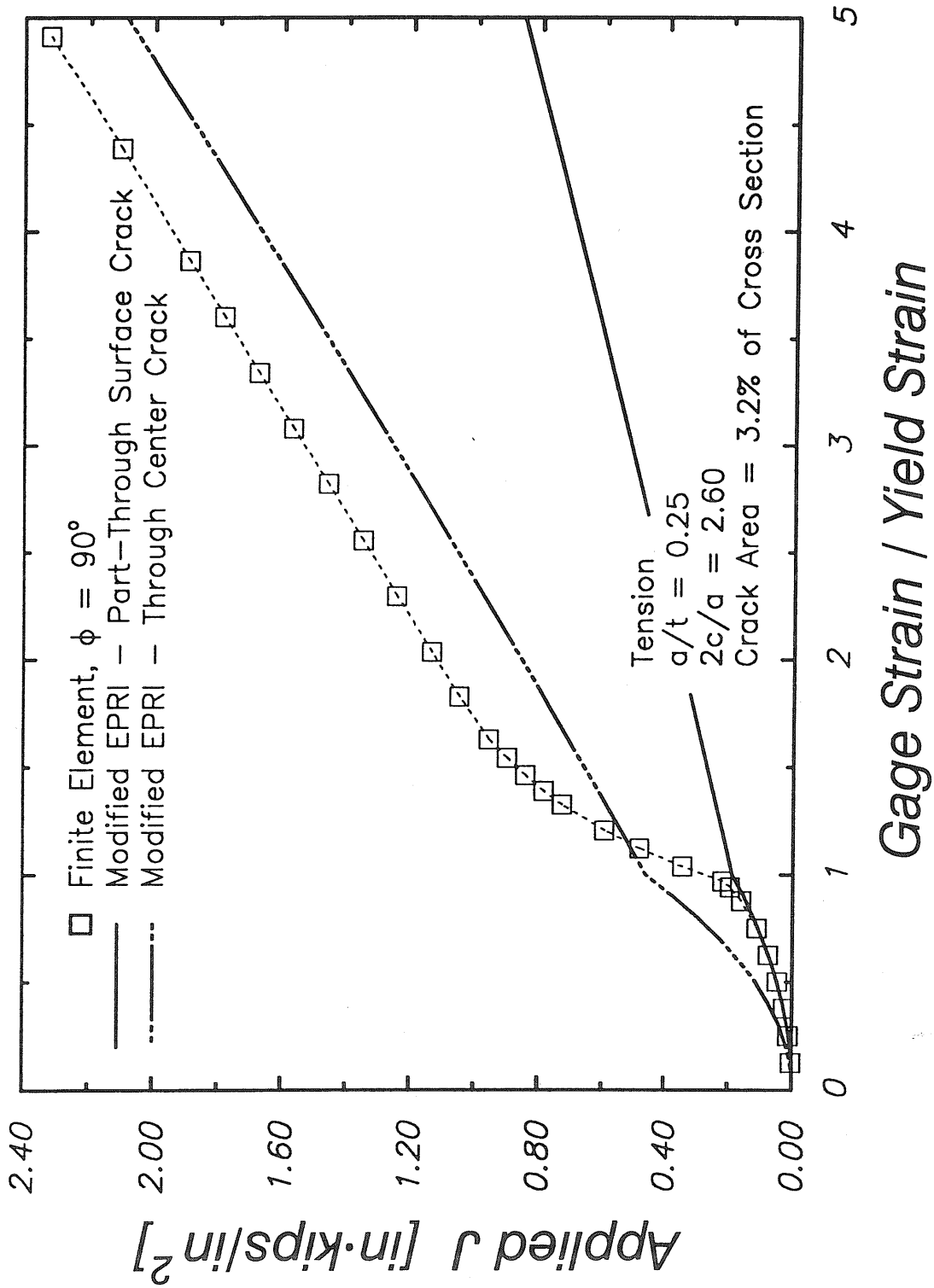

Figure 16(a): Comparison of through and part–through crack approximations using the modified EPRI approach to the finite element results for Crack 2 loaded by remote tension.

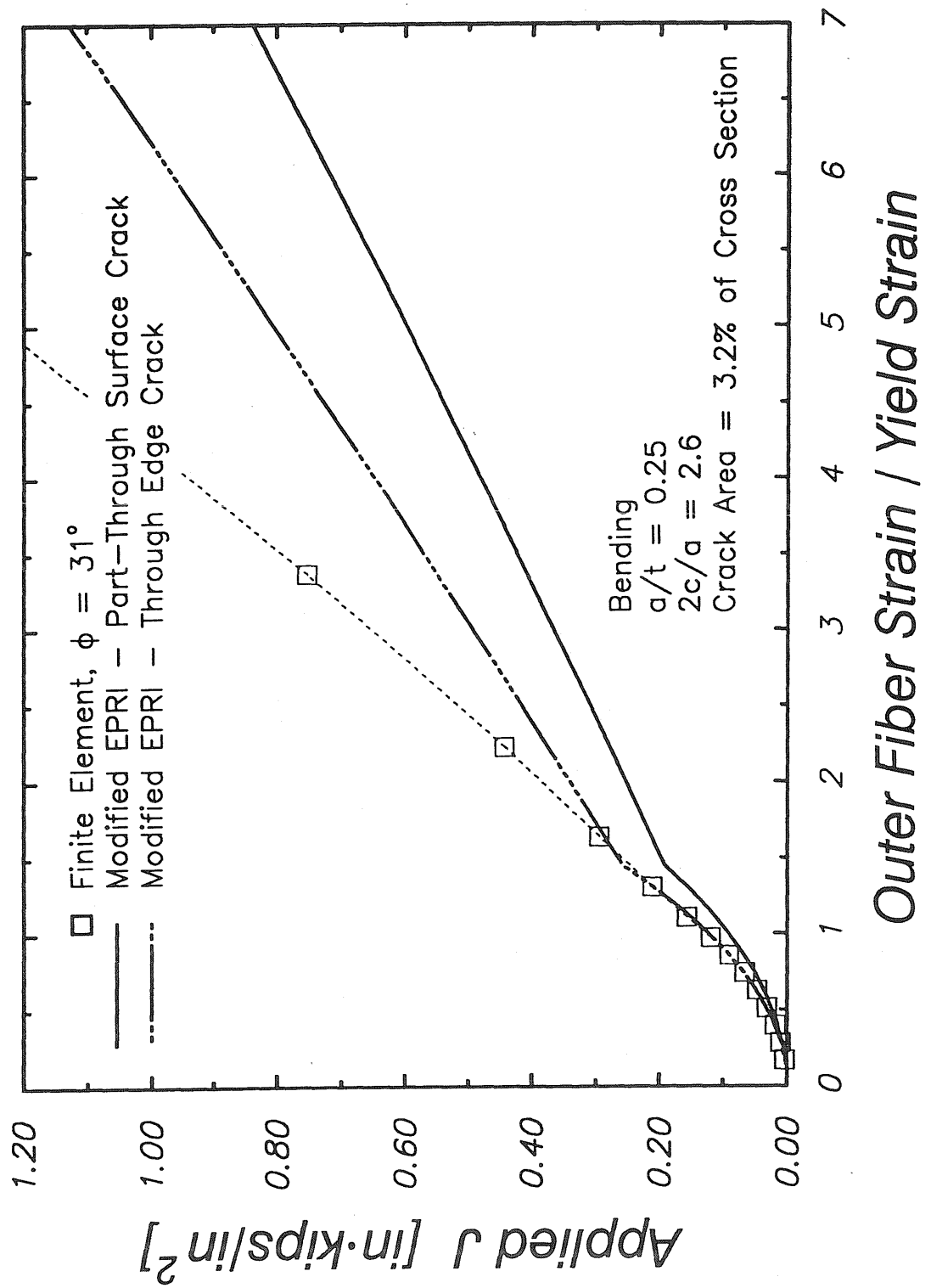

Figure 16(b): Comparison of through and part–through crack approximations using the modified EPRI approach to the finite element results for Crack 2 loaded by remote bending.

6. REFERENCES

[1] Bhandari, S., et al., "Establishment of Governing Parameters for Fatigue Crack Growth Analysis in Areas of High Nominal Strain," ASME Paper 84–PVP–20, 1984.

[2] Marriott, D.L., "Efficient Representation of Fracture Mechanics Knowledge for Design Application," presented at the Institute of Metals Conference on Materials and Engineering Design, London, 1988.

[3] Ainsworth, R.A., "The Assessment of Defects in Structures of Strain Hardening Material," *Engineering Fracture Mechanics*, Vol. 19, No. 4, pp. 633–642, 1984.

[4] Penny, R.K., and Marriott, D.L., *Design for Creep*, McGraw–Hill, New York, 1971.

[5] Kumar, V., German, M.D., and Shih, C.F., "An Engineering Approach for Elastic–Plastic Fracture Analysis," EPRI Report NP–1931, Electric Power Research Institute, 1981.

[6] Miller, A.G., "Review of Limit Loads of Structures Containing Defects," *International Journal of Pressure Vessels and Piping*, Vol. 32, pp. 197–327, 1988.

[7] Tada, H., Paris, P.C., and Irwin, G.C., *The Stress Analysis of Cracks Handbook*, Del Research Corporation, 1985.

[8] Newman, J.C., and Raju, I.S., "Stress Intensity Factors for Cracks in Three Dimensional Finite Bodies Subjected to Tension and Bending Loads," NASA Technical Memorandum No. 85793, 1984.

[9] Turner, C.E., "Further Developments of a J–Based Design Curve and its Relationship to Other Procedures," *Elastic–Plastic Fracture: Second Symposium, Volume II – Fracture Resistance Curves and Engineering Applications, ASTM STP 803*, C.F. Shih and J.P. Gudas, Eds., pp. II–80–II–102, 1983.

[10] Dodds, R.H., Anderson, T.L., and Kirk, M.T., "Numerical Correlation of Size Effects on Elastic–Plastic Fracture Toughness (J_c) in SENB Specimens," to appear in the *International Journal of Fracture.*

[11] Dodds, R.H., and Lopez, L.A., "Software Virtual Machines for Development of Finite–Element Systems," *International Journal for Engineering with Computers*, Vol. 13, pp. 18–26, 1985.

[12] Bass, B.R., and Bryson, J.W., "Applications of Energy Release Rate Techniques to Part-Through Cracks in Plates and Cylinders. Volume 1. ORMGEN-3D.," NUREG/CR-2997, ORNL/TM-8527/V1.

[13] Dodds, R., "Numerical Techniques for Plasticity Computations in Finite Element Analysis," *Computers and Structures,* Vol. 5, pp. 767-779, 1987.

[13] PATRAN User's Manual, Release 2.3. PDA Engineering, Inc., Costa Mesa, CA, 1989.

[14] Simo, J.C., and Taylor, R.L., "Consistent Tangent Operators for Rate-Independent Elastoplasticty," *Computer Methods in Applied Mechanics and Engineering*, Vol. 48, pp. 1101-1118, 1985.

[16] Rice, J.R., "A Path Independent Integral and the Approximate Analysis of Strain Concentrations by Notches and Cracks," *Journal of Applied Mechanics*, Vol. 35, pp. 379-386, 1968.

[15] Eshelby, J.D., "Energy Relations and the Energy Momentum Tensor in Continuum Mechanics," *Inelastic Behavior of Solids,* M.F. Kanninen, et al., Eds., Mc Graw-Hill, NY, 1970.

[17] Li, F.Z., Shih, C.F., and Needleman, A., "A Comparison of Methods for Calculating Energy Release Rates," *Engineering Fracture Mechanics*, Vol. 21, pp. 405-421, 1985.

[18] Shih, C.F., Moran, B., and Nakamura, T., "Energy Release Rate Along a Three-Dimensional Crack Front in a Thermally Stressed Body," *International Journal of Fracture*, Vol. 30, pp. 79-102, 1986.

[19] Raju, I.S., and Newman, J.C., "Stress-Intensity Factors for a Wide Range of Semi-Elliptical Surface Cracks in Finite-Thickness Plates," *Engineering Fracture Mechanics,* Vol. 11, pp. 817-829, 1979.

[20] Miller, A.G., and Ainsworth, R.A., "Consistency of Numerical Results for Power-Law hardening Materials and the Accuracy of the Reference Stress Approximation for *J*," *Engineering Fracture Mechanics*, Vol. 32, No. 2, pp. 233-247, 1989.

[21] Dodds, R.H., and Read, D.T., "Experimental and Numerical Studies for the J-Integral for a Surface Flaw," *International Journal of Fracture*, Vol. 43, pp. 47-67, 1990.

APPENDIX A

Tables in this appendix document the variation of J with applied strain and location around the crack front (ϕ) determined by finite element analysis. The circular angle ϕ is defined in Figure 3; $\phi = 90°$ designates the crack front position of maximum depth while $\phi = 0°$ designates the intersection of the crack front with the free surface of the plate.

Table A1: Variation of J with Applied Load for Crack #1 Loaded in Tension.										
Remote Stress [ksi]	$\phi=90$ CMOD [mills]	e / e_y	J at $\phi=90$	J at $\phi=73.4$	J at $\phi=59.2$	J at $\phi=45$	J at $\phi=30.8$	J at $\phi=16.6$	J at $\phi=2.37$	J at $\phi=0$
20.00	0.632	0.250	0.005	0.005	0.005	0.005	0.005	0.005	0.005	0.005
30.00	0.948	0.375	0.012	0.013	0.012	0.012	0.012	0.012	0.012	0.011
40.00	1.272	0.500	0.023	0.023	0.022	0.021	0.021	0.021	0.022	0.016
50.00	1.598	0.625	0.035	0.036	0.035	0.034	0.033	0.033	0.033	0.028
60.00	1.944	0.750	0.053	0.054	0.053	0.052	0.051	0.051	0.047	0.034
70.00	2.320	0.875	0.076	0.078	0.077	0.075	0.074	0.073	0.064	0.044
75.00	2.550	0.937	0.091	0.094	0.092	0.090	0.089	0.086	0.074	0.050
77.00	2.670	0.962	0.099	0.101	0.100	0.098	0.096	0.093	0.079	0.051
79.00	2.836	0.988	0.109	0.112	0.111	0.109	0.107	0.103	0.086	0.056
79.50	2.922	0.995	0.114	0.118	0.116	0.114	0.112	0.108	0.090	0.058
79.75	3.086	1.002	0.125	0.128	0.127	0.125	0.122	0.117	0.096	0.061
80.00	3.754	1.051	0.166	0.171	0.169	0.165	0.160	0.150	0.120	0.073
80.10	4.230	1.126	0.194	0.198	0.196	0.192	0.185	0.171	0.135	0.080
80.20	4.522	1.231	0.211	0.216	0.214	0.209	0.201	0.184	0.145	0.086
80.30	4.840	1.335	0.230	0.235	0.232	0.227	0.217	0.198	0.156	0.089
80.40	5.156	1.439	0.248	0.254	0.251	0.245	0.234	0.212	0.166	0.096
80.60	5.790	1.647	0.286	0.292	0.288	0.281	0.267	0.238	0.186	0.108
80.80	6.422	1.856	0.324	0.329	0.325	0.315	0.298	0.266	0.207	0.117
81.05	7.216	2.116	0.372	0.377	0.372	0.360	0.338	0.298	0.232	0.133
81.30	8.008	2.377	0.421	0.427	0.420	0.405	0.377	0.330	0.256	0.152
81.55	8.796	2.638	0.468	0.473	0.465	0.447	0.417	0.367	0.284	0.158
81.80	9.586	2.899	0.517	0.523	0.513	0.491	0.456	0.399	0.308	0.179
82.05	10.376	3.160	0.568	0.573	0.561	0.536	0.495	0.432	0.331	0.200
82.30	11.164	3.421	0.619	0.624	0.610	0.581	0.534	0.465	0.355	0.222
82.55	11.936	3.683	0.663	0.669	0.653	0.623	0.576	0.506	0.386	0.216
83.05	13.504	4.204	0.764	0.769	0.748	0.710	0.653	0.572	0.435	0.254
83.55	15.072	4.730	0.867	0.872	0.845	0.798	0.732	0.641	0.485	0.286

Note: J is in in•kips/in^2
a = 0.26–inches 2c = 0.68–inches
t = 2–inches 2b = 8–inches
a/t = 0.13 2c/a = 2.62
Crack Area / Ligament Area = 0.009

Table A2: Variation of J with Applied Load for Crack #1 Loaded in Bending.										
Applied Moment [kip–in]	$\phi = 90$ CMOD [mills]	e / e_y	J at $\phi = 90$	J at $\phi = 73.4$	J at $\phi = 59.2$	J at $\phi = 45$	J at $\phi = 30.8$	J at $\phi = 16.6$	J at $\phi = 2.37$	J at $\phi = 0$
50	0.560	0.221	0.003	0.003	0.003	0.003	0.003	0.004	0.004	0.004
100	1.124	0.443	0.013	0.014	0.014	0.014	0.014	0.016	0.017	0.014
150	1.700	0.664	0.031	0.031	0.031	0.032	0.034	0.037	0.037	0.027
200	2.312	0.887	0.056	0.057	0.058	0.060	0.064	0.068	0.063	0.041
250	3.096	1.146	0.096	0.099	0.102	0.106	0.111	0.114	0.099	0.056
300	4.662	1.722	0.184	0.189	0.194	0.201	0.211	0.209	0.168	0.085
320	5.870	2.207	0.245	0.252	0.260	0.273	0.289	0.282	0.222	0.107
340	7.856	2.968	0.343	0.354	0.371	0.398	0.426	0.405	0.312	0.140
350	9.488	3.582	0.426	0.439	0.465	0.504	0.540	0.507	0.385	0.167
360	12.088	4.541	0.557	0.576	0.618	0.677	0.724	0.671	0.503	0.208
370	16.172	6.052	0.764	0.793	0.863	0.952	1.016	0.930	0.687	0.269
380	21.400	8.199	1.058	1.104	1.210	1.341	1.432	1.299	0.947	0.353
390	29.320	10.955	1.434	1.503	1.656	1.839	1.966	1.768	1.275	0.456

Note: J is in in•kips/in^2
a = 0.26–inches 2c = 0.68–inches
t = 2–inches 2b = 8–inches
a/t = 0.13 2c/a = 2.62
Crack Area / Ligament Area = 0.009

Table A3: Variation of J with Applied Load for Crack #2 Loaded in Tension.										
Remote Stress [ksi]	$\phi=90$ CMOD [mills]	e / e_y	J at $\phi=90$	J at $\phi=73.4$	J at $\phi=59.2$	J at $\phi=45$	J at $\phi=30.8$	J at $\phi=16.6$	J at $\phi=2.37$	J at $\phi=0$
10.00	0.622	0.125	0.002	0.002	0.002	0.002	0.002	0.002	0.002	0.002
20.00	1.247	0.250	0.011	0.011	0.011	0.010	0.010	0.010	0.011	0.010
30.00	1.879	0.375	0.026	0.025	0.025	0.024	0.023	0.024	0.025	0.020
40.00	2.521	0.501	0.046	0.046	0.045	0.043	0.042	0.043	0.045	0.032
50.00	3.181	0.626	0.074	0.073	0.072	0.070	0.068	0.070	0.069	0.045
60.00	3.875	0.751	0.110	0.109	0.107	0.105	0.103	0.104	0.097	0.059
70.00	4.666	0.877	0.159	0.158	0.156	0.153	0.151	0.149	0.132	0.077
75.00	5.222	0.941	0.196	0.195	0.192	0.190	0.187	0.183	0.158	0.091
77.00	5.586	0.969	0.219	0.219	0.217	0.214	0.212	0.205	0.175	0.101
79.00	7.546	1.036	0.345	0.345	0.344	0.342	0.338	0.317	0.258	0.145
79.50	9.654	1.120	0.482	0.481	0.478	0.472	0.459	0.417	0.331	0.180
79.75	11.417	1.205	0.593	0.592	0.588	0.578	0.556	0.495	0.389	0.209
80.00	13.552	1.325	0.727	0.725	0.720	0.705	0.669	0.586	0.458	0.245
80.10	14.466	1.388	0.784	0.783	0.777	0.759	0.717	0.626	0.488	0.261
80.20	15.388	1.461	0.842	0.841	0.834	0.813	0.765	0.665	0.518	0.278
80.30	16.301	1.542	0.900	0.898	0.891	0.867	0.813	0.704	0.547	0.295
80.40	17.190	1.628	0.956	0.955	0.946	0.918	0.858	0.743	0.576	0.312
80.60	18.648	1.828	1.050	1.048	1.037	1.004	0.936	0.809	0.626	0.342
80.80	19.990	2.036	1.136	1.134	1.121	1.084	1.009	0.871	0.673	0.371
81.05	21.661	2.296	1.245	1.242	1.226	1.183	1.100	0.950	0.732	0.403
81.30	23.321	2.556	1.352	1.349	1.330	1.282	1.192	1.029	0.792	0.434
81.55	24.978	2.817	1.460	1.456	1.435	1.381	1.283	1.109	0.851	0.469
81.80	26.623	3.078	1.569	1.564	1.539	1.480	1.374	1.188	0.911	0.497
82.05	28.270	3.340	1.675	1.670	1.642	1.577	1.465	1.266	0.968	0.535
82.30	29.906	3.602	1.784	1.777	1.745	1.675	1.556	1.347	1.030	0.561
82.55	31.542	3.863	1.892	1.885	1.850	1.774	1.648	1.427	1.092	0.589
83.05	34.781	4.387	2.103	2.093	2.052	1.967	1.829	1.580	1.196	0.667
83.55	38.013	4.911	2.319	2.306	2.258	2.164	2.014	1.741	1.320	0.719

Note: J is in in•kips/in^2
a = 0.50–inches 2c = 1.30–inches
t = 2–inches 2b = 8–inches
a/t = 0.25 2c/a = 2.60
Crack Area / Ligament Area = 0.032

Table A4: Variation of J with Applied Load for Crack #2 Loaded in Bending.										
Applied Moment [kip–in]	$\phi = 90$ CMOD [mills]	e / e_y	J at $\phi = 90$	J at $\phi = 73.4$	J at $\phi = 59.2$	J at $\phi = 45$	J at $\phi = 30.8$	J at $\phi = 16.6$	J at $\phi = 2.37$	J at $\phi = 0$
75.0	0.773	0.170	0.002	0.002	0.002	0.003	0.003	0.003	0.004	0.004
125.1	1.291	0.284	0.007	0.007	0.007	0.008	0.009	0.010	0.012	0.012
175.1	1.811	0.398	0.013	0.014	0.015	0.016	0.018	0.021	0.025	0.021
225.1	2.335	0.512	0.022	0.023	0.024	0.027	0.030	0.036	0.041	0.031
275.2	2.867	0.626	0.034	0.035	0.037	0.040	0.046	0.054	0.060	0.041
325.2	3.408	0.740	0.048	0.049	0.052	0.057	0.065	0.077	0.081	0.052
375.3	3.964	0.855	0.064	0.066	0.070	0.078	0.089	0.105	0.105	0.064
425.3	4.546	0.970	0.084	0.086	0.093	0.103	0.118	0.136	0.132	0.077
475.3	5.221	1.105	0.110	0.113	0.122	0.136	0.156	0.175	0.163	0.093
525.3	6.154	1.309	0.151	0.156	0.168	0.187	0.211	0.231	0.207	0.114
575.4	7.522	1.638	0.219	0.225	0.241	0.264	0.295	0.313	0.270	0.143
625.4	9.856	2.230	0.342	0.349	0.369	0.401	0.443	0.455	0.379	0.188
675.4	14.512	3.368	0.569	0.582	0.619	0.680	0.753	0.749	0.598	0.272
725.5	27.835	6.579	1.197	1.240	1.366	1.544	1.692	1.631	1.231	0.491
749.8	40.602	9.634	1.800	1.886	2.118	2.399	2.619	2.499	1.833	0.683

Note: J is in in•kips/in^2
a = 0.50–inches 2c = 1.30–inches
t = 2–inches 2b = 8–inches
a/t = 0.25 2c/a = 2.60
Crack Area / Ligament Area = 0.032

Table A5: Variation of J with Applied Load for Crack #3 Loaded in Tension.										
Remote Stress [ksi]	$\phi=90$ CMOD [mills]	e / e_y	J at $\phi=90$	J at $\phi=73.4$	J at $\phi=59.2$	J at $\phi=45$	J at $\phi=30.8$	J at $\phi=16.6$	J at $\phi=2.37$	J at $\phi=0$
10.00	0.860	0.125	0.005	0.005	0.005	0.004	0.003	0.003	0.002	0.002
20.00	1.727	0.251	0.021	0.021	0.019	0.016	0.013	0.010	0.009	0.009
30.00	2.609	0.378	0.049	0.047	0.043	0.037	0.030	0.024	0.021	0.018
40.00	3.515	0.504	0.087	0.085	0.078	0.068	0.055	0.044	0.038	0.028
50.00	4.458	0.630	0.139	0.135	0.124	0.108	0.089	0.072	0.061	0.040
60.00	5.490	0.757	0.206	0.201	0.185	0.163	0.137	0.112	0.091	0.055
70.00	6.875	0.887	0.304	0.297	0.277	0.249	0.214	0.178	0.138	0.079
75.00	8.804	0.971	0.439	0.432	0.410	0.378	0.334	0.277	0.205	0.113
77.00	12.039	1.059	0.666	0.658	0.632	0.587	0.519	0.420	0.297	0.155
78.00	15.706	1.163	0.935	0.922	0.881	0.812	0.709	0.560	0.385	0.194
78.50	19.048	1.270	1.188	1.168	1.108	1.009	0.868	0.671	0.453	0.225
79.00	23.610	1.425	1.535	1.506	1.420	1.279	1.079	0.813	0.538	0.269
79.50	29.182	1.630	1.959	1.920	1.800	1.603	1.328	0.979	0.638	0.326
80.00	35.463	1.894	2.435	2.382	2.221	1.962	1.606	1.163	0.750	0.394
80.25	38.724	2.060	2.683	2.623	2.442	2.151	1.752	1.262	0.811	0.432
80.50	41.990	2.244	2.930	2.864	2.664	2.340	1.900	1.362	0.872	0.471
80.75	45.179	2.443	3.173	3.100	2.881	2.527	2.046	1.463	0.935	0.510

Note: J is in in•kips/in^2
a = 0.50–inches 2c = 3.00–inches
t = 2–inches 2b = 8–inches
a/t = 0.25 2c/a = 6.00
Crack Area / Ligament Area = 0.074

Table A6: Variation of J with Applied Load for Crack #3 Loaded in Bending.

Applied Moment [kip-in]	$\phi=90$ CMOD [mills]	e / e_y	J at $\phi=90$	J at $\phi=73.4$	J at $\phi=59.2$	J at $\phi=45$	J at $\phi=30.8$	J at $\phi=16.6$	J at $\phi=2.37$	J at $\phi=0$
75.0	1.048	0.179	0.005	0.005	0.005	0.005	0.004	0.004	0.004	0.004
125.0	1.751	0.299	0.014	0.014	0.014	0.014	0.013	0.011	0.011	0.010
175.0	2.459	0.419	0.028	0.028	0.028	0.027	0.025	0.022	0.021	0.018
225.0	3.174	0.540	0.047	0.047	0.046	0.044	0.041	0.037	0.036	0.027
275.0	3.899	0.661	0.070	0.070	0.069	0.066	0.062	0.056	0.053	0.037
325.0	4.636	0.782	0.098	0.097	0.096	0.093	0.087	0.080	0.074	0.047
375.0	5.392	0.905	0.130	0.130	0.128	0.125	0.118	0.110	0.098	0.059
425.0	6.184	1.031	0.168	0.168	0.167	0.163	0.156	0.146	0.125	0.072
475.0	7.141	1.210	0.219	0.219	0.218	0.215	0.207	0.193	0.160	0.089
525.0	8.476	1.487	0.294	0.295	0.295	0.292	0.282	0.260	0.208	0.112
575.0	10.577	1.967	0.421	0.422	0.423	0.418	0.401	0.364	0.283	0.145
625.0	14.819	2.865	0.680	0.681	0.678	0.666	0.639	0.577	0.434	0.210
675.0	24.259	4.804	1.273	1.272	1.265	1.242	1.188	1.048	0.759	0.341
700.0	34.935	6.988	1.979	1.980	1.972	1.933	1.836	1.598	1.134	0.492
725.0	51.822	10.427	3.121	3.125	3.125	3.058	2.884	2.497	1.743	0.735

Note: J is in in•kips/in^2
a = 0.50–inches 2c = 3.00–inches
t = 2–inches 2b = 8–inches
a/t = 0.25 2c/a = 6.00
Crack Area / Ligament Area = 0.074